STRUCTURAL DYNAMIC CHARACTERISTICS OF TRANSMISSION SYSTEMS

by

Rajendra K. Mathur

A thesis
presented to the University of Manitoba
in partial fulfillment of the
requirements for the degree of
MASTER OF SCIENCE
in
CIVIL ENGINEERING DEPARTMENT

Winnipeg, Manitoba

STRUCTURAL DYNAMIC CHARACTERISTICS OF TRANSMISSION SYSTEMS

BY

RAJENDRA KARAN MATHUR

A thesis submitted to the Faculty of Graduate Studies of
the University of Manitoba in partial fulfillment of the requirements
of the degree of

MASTER OF SCIENCE

ABSTRACT

An algorithm to perform the free vibration analysis of a transmission tower system has been developed. The algorithm is designed to be a general purpose package which is suitable for a micro-computer. Therefore, the support structures may be free-standing or guy-supported, lattice or non-lattice.

The finite element method has been employed to model the interactive components of the towers, guys, insulators and conductors. Both lattice or non-lattice tower segments have been idealized as beam elements with a consistent mass matrix. The effects of axial load have been incorporated in the element by using a geometric stiffness matrix. However, a lattice tower usually contains tapered segments. Therefore, the stiffness and consistent mass matrices were derived by employing the exact displacement function for an equivalent tapered beam loaded only at its ends. Also, a specialized finite element has been developed to represent the transverse vibrations of an inclined cable. It was assumed that the cable follows a parabolic profile when it hangs under its own weight. This element has been used to model both guy-wires and conductors.

The free-vibration analysis of a free-standing lattice tower has been performed. The idealized model gave comparable results with those obtained from a structural analysis package known as SAPIV. However, the input is much more complicated with SAPIV and many more elements are required. Natural frequencies obtained by using the finite element model for a horizontal cable were comparable with analytical results. Finally, the algorithm was employed to perform a detailed free-vibration analysis of a two-span transmission line with guyed supporting structures. The effect of swinging of the insulator on the tower/conductor interaction has been studied. The low frequency modes primarily involved conductor motion so that the conductor may be excited with large amplitudes in a condition known as galloping. By assuming a feasible amplitude of galloping, an estimation has been made of the load transferred to the tower. It was noticed that the swinging of the insulators significantly decreased the horizontal(along-line) loads due to galloping. Also, static coupling with remote conductor spans was considered. It was found that such coupling significantly reduced the vertical loads on the central tower.

ACKNOWLEDGEMENT

I wish to express my sincere thanks to Professors A. Shah, N. Popplewell and R. B. Pinkney for their continuous guidance and encouragement throughout this work. The invaluable assistance rendered by Mr. P. G. S. Trainor is deeply appreciated. Finally, the author wishes to thank the Manitoba HVDC Research Centre for financial support.

CONTENTS

LIST OF FIGURES

LIST OF TABLES

Chapter I

INTRODUCTION

1.1 General Introduction

Severe freezing rain storms are not uncommon during winter months. Such storms have resulted in extensive damage to transmission and communication tower systems. For instance, nine transmission towers collapsed completely south of Oakville, Manitoba during an ice storm on April 27, 1984. The failure was due to heavy ice build-up on the conductor and towers in conjunction with moderate winds. Similar failures have been experienced with communication tower systems which are generally guy supported.

A contributing factor in a collapse is that most designs are based on a static analysis so that dynamic loads are invariably ignored. This practice is due to the extreme difficulty of studying the dynamic behaviour of complicated structures, either experimentally or analytically. However, the increased availability of computer facilities will promote the inclusion of a dynamic analysis in future designs of towers. In general, a tower system can be loaded dynamically by earthquakes, longitudinal impact due to gusty winds, unbalanced tension in the line and a broken cable

usually caused by icing [1]. In addition, one of the most common causes of dynamic loading is the galloping of iced cables. Galloping is the wind-induced excitation of the low frequency modes of a cable to large amplitudes of vibration [2]. The energy transfer has the form of a negative viscous damping and does not usually occur unless the cable is iced.

The initial objective of a dynamic analysis is to calculate a tower system's natural frequencies. These frequencies may be then employed to estimate, for example, the tower's peak response to a gusty wind, the impact caused by conductor breakage or the forces on the tower due to cables in gallop.

In this thesis, the free vibration analysis of a tower system will be performed. The basic element of the tower system can be either a lattice or a non-lattice structure. This supporting structure can be either free standing as shown in Figure 1.1 or guy-supported as in Figure 4.1. An algorithm will be developed to accommodate both types of structure on a microcomputer.

1.2 Free-Vibration Analysis

The dynamic stiffness, $K(\omega)$, for a beam and a cable element are available in references [3] and [4], respectively. These stiffnesses are functions of the natural frequencies, ω_n. They can be used potentially to obtain an analytical

solution of a forced-vibration analysis. However, the use of a dynamic stifffness in a free vibration analysis leads to an equation of the form $\det|K(\omega)| = 0$. This equation contains transcendental functions which are trignometric and hyperbolic expressions involving ω_n [5]. The solution of such an equation can be obtained by using the incremental search method [6]. However, there is a chance of missing some particular natural frequencies because of the highly variable nature of $K(\omega)$. It is much simpler and more reliable to construct a finite element model and solve the eigenvalue problem in the form $(K - \omega^2 M)\, a = 0$. Here the assembled stiffness matrix [K] and mass matrix [M] are independent of ω_n. The eigenvalue solution will give a reasonable approximation to the lower natural frequencies of a system without skipping roots. The accuracy of the results can be increased by choosing a larger number of elements. The eigenvector corresponding to each eigenvalue represents the deflected shape of the system vibrating at a particular natural frequency. Convenient finite element representations for masts and cables will be developed in this thesis and their modelling will be tested by using practical examples.

A procedure will be developed in Chapter II to generate stiffness and mass matrices for typical tower body sections. Specifically, uniform lattice, tapered lattice and prismatic structural sections will be considered. In Chapter III, the stiffness and mass matrices for an inclined cable element

will be generated. A detailed analysis of the transmission tower system shown in Figure 4.1 will be presented in Chapter IV. From the results, an estimation of the loads transferred to the tower in the event of galloping will be given. Also, the effects of such factors as axial loads on the towers, and insulator swing will be discussed.

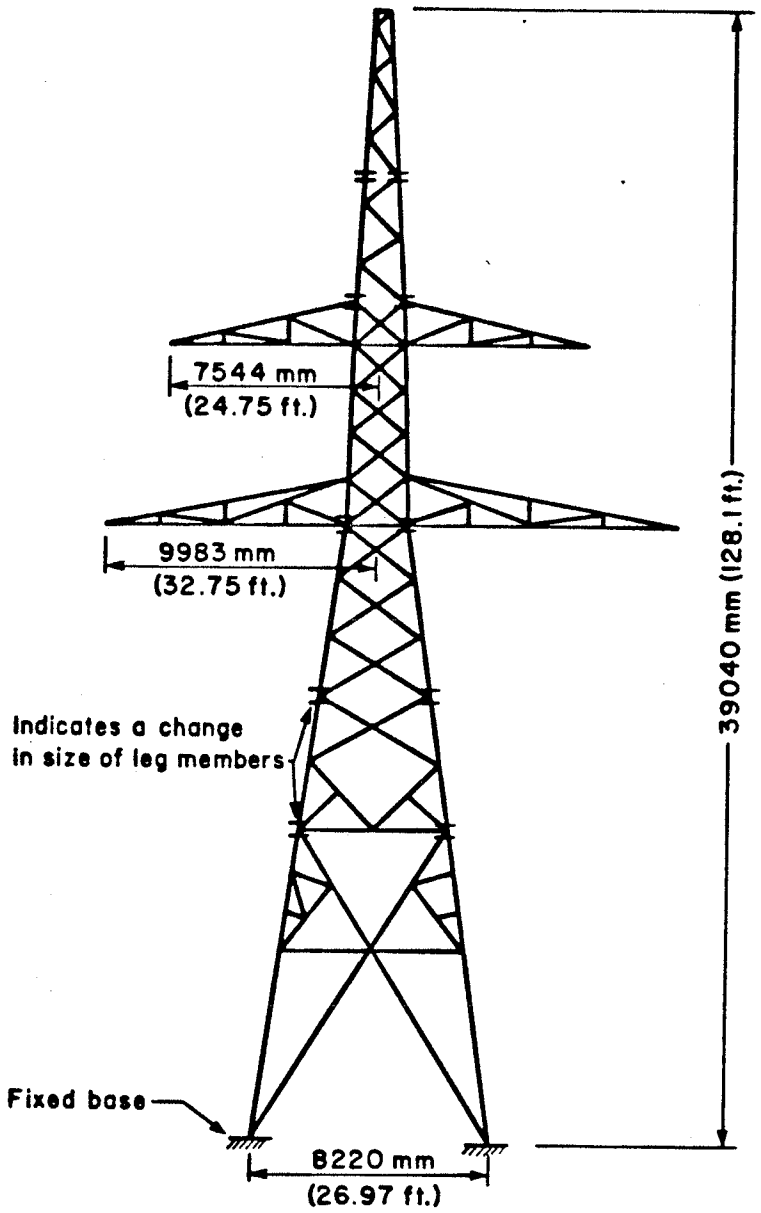

Figure 1.1: Typical Free-standing Lattice Tower.

Chapter II

FINITE ELEMENT MODELLING

2.1 Introduction

The Finite element modelling of the segment of a tower's body will be developed in this chapter. Specifically, the type of elements which will be considered are:

1. straight prismatic segments such as rectangular or circular tubes; and,
2. lattice segments which may be either tapered or straight.

It is well known that prismatic elements can be modelled straightforwardly as beam elements, which resist bending, torsional and axial loads [7]. The resulting twelve-by-twelve stiffness and consistent mass matrices for one such element are given in books [8] and, for reference, in Appendix A. A geometric stiffness is also included to account for axial loads on the tower and is as given in Appendix A. This latter stiffness modifies the conventional stiffness matrix and generally reduces the flexural natural frequencies [9].

The development of mass and stiffness for a tapered lattice structure is not straightforward. One approach is to

employ a space-frame model using a computer analysis package such as SAPIV [10]. However, each and every leg or bracing member must be represented, so that preparation of the computer input is very tedious and requires very careful checking. Also, the number of degrees of freedom in a space-frame model is very large (typically 1000-2000) and, consequently, there may be problems associated with the availability of computer storage and time.

The aim here is to circumvent the above problems and produce a tower analysis package which is suitable for use on a micro-computer. The approach is based on the assumption that the typical tapered lattice segment shown in Figure 2.1 can be represented approximately by an equivalent tapered beam [7,11]. It will be shown that then the stiffness and consistent mass matrices can be easily developed, based on an assumed mode shape. It will be shown that the solution for the equilibrium equation for a tapered beam element is a logarithmic function. Such a solution, however, leads to a complicated procedure for obtaining the mode shapes and, eventually, the stiffness and mass matrices. To avoid this complication and thereby develop an efficient computational approach, a simple cubic polynomial will be assumed. This polynomial happens to be the exact solution of the equilibrium equation for a straight beam. Although the cubic polynomial will be demonstrated to be computationally efficient for straight beams, it will be shown to fail

for tapered beams. Hence both, the cubic polynomial and logarithmic expressions will be employed for the generation of stiffness and mass matrices, depending upon the type of beam considered.

This procedure will be illustrated in detail for the case of the bending of beam elements.

2.2 Tapered beam representation of a latticed structure

2.2.1 Bending

A Typical tapered lattice segment has a square cross section. It is supported by four continuous legs, each having a

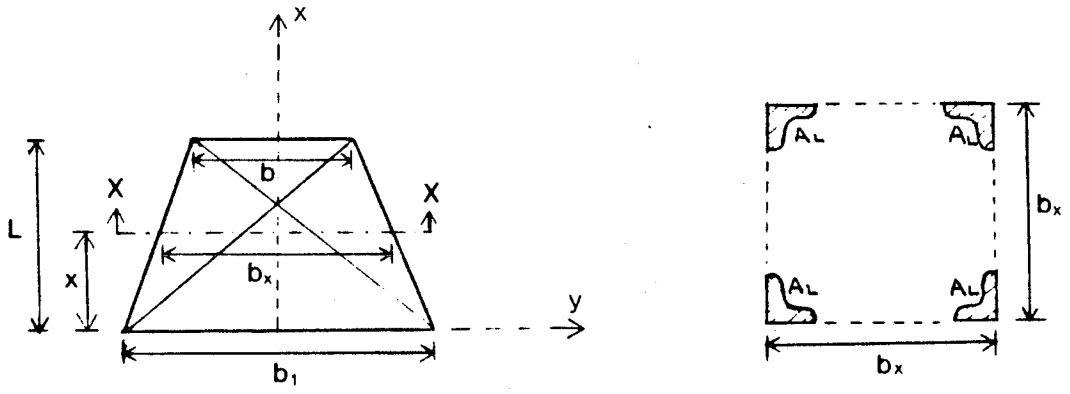

(a) (b)

Figure 2.1 (a): Typical Tapered segment
(b): Plan-view at section X-X .

cross-sectional area A_L as shown in Figure 2.1(a) and 1(b).

The moment of inertia, I(x), about the segment's longitudinal axis x, at section X-X, is given by equation [12]

$$I(x) = A_L\, b_x^2 \qquad (2.1a)$$

in which $b_x = b_1(1 - \beta x)$ (2.1b)

$$\text{and} \qquad \beta = \frac{b_1 - b}{b_1 L} \tag{2.1c}$$

$$\text{hence } I(x) = A_L b_1^2 (1 - \beta x)^2 \tag{2.2a}$$

$$\text{or} \quad I(x) = I_0 (1 - \beta x)^2 \tag{2.2b}$$

where I_0 is the moment of inertia at the base of the segment.

Now the area of each leg, A_L, is constant along the length of the segment, so that the mass per unit length of the segment, m_0, is also constant.

The next step is to develop the stiffness and consistent mass matrices for the typical beam element shown in Figure 2.2. The generalized coordinates v_1, v_2, v_3 and v_4 are the end displacements and slopes as shown in the figure and the

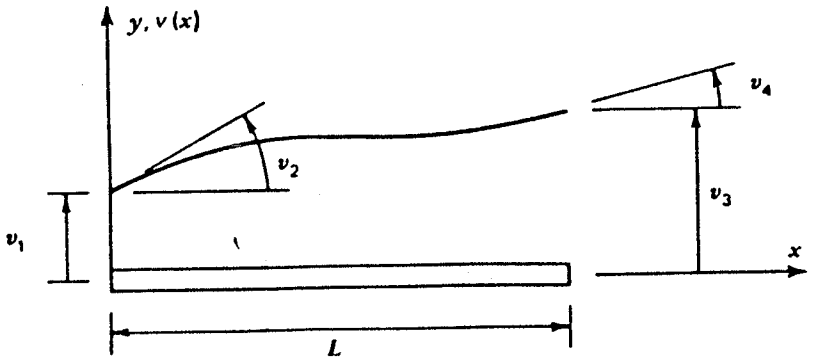

Figure 2.2: An element undergoing transverse deflection

mode shape is v(x).

The element's stiffness matrix [K] is derived from the expression of strain energy [8]

$$U = \frac{1}{2}\int_0^L EI(v'')^2 \, dx = \frac{1}{2} \{V\}^T [K] \{V\} \tag{2.3a}$$

$$\text{where } \{V\} = \langle v_1 \quad v_2 \quad v_3 \quad v_4 \rangle^T . \tag{2.3b}$$

Similarly, the consistent mass matrix, [M], is obtained from the expression for kinetic energy, T, which is

$$T = \frac{1}{2}\int_0^L m\dot{v}^2\,dx = \frac{1}{2}\{\dot{V}\}^T[M]\{\dot{V}\} \quad . \tag{2.4}$$

An appropriate mode shape can be chosen from the equilibrium equation

$$(EI(x)\,v'')'' = 0 \tag{2.5}$$

for a beam element loaded only at its ends.
Substituting relation (2.2b) into equation(2.5) and integrating gives

$$v(x) = C_1 Ln(1 - \beta x) + C_2(1 - \beta x)Ln(1 - \beta x) + C_3(1 - \beta x) + C_4 \tag{2.6}$$

in which C_1 through C_4 are constants.

This function represents the exact static deflection for a tapered beam. However, it leads to a procedure which is rather cumbersome for use in the finite element method. Generally it is desirable to minimize computational effort, especially if the method is to be suitable for a micro-computer. A much simpler but more computationally efficient alternative is to use the cubic relation

$$v(x) = B_1 + B_2(x/L) + B_3(x/L)^2 + B_4(x/L)^3 \tag{2.7}$$

which happens to be the static deflection for a uniform beam. Therefore, the accuracy and efficiency of finite element computations based on the alternative mode shapes will be considered.

The generation of the stiffness and mass matrices by using relation (2.7) is straightforward and similar to that shown in reference [8]. Firstly, let

$$v(x) = \psi_1 v_1 + \psi_2 v_2 + \psi_3 v_3 + \psi_4 v_4 \tag{2.8}$$

where ψ_1 through ψ_4 are independent cubic polynomials. Hence, since $v(0) = v_1$, $v'(0) = v_2$, $v(L) = v_3$, $v'(L) = v_4$ then

$$\begin{aligned} &\psi_1(0) = 1,\ \psi_1'(0) = \psi_1(L) = \psi_1'(L) = 0 \\ &\psi_2'(0) = 1,\ \psi_2(0) = \psi_2(L) = \psi_2'(L) = 0 \\ &\psi_3(L) = 1,\ \psi_3(0) = \psi_3'(0) = \psi_3'(L) = 0 \quad \text{and} \\ &\psi_4'(L) = 1,\ \psi_4(0) = \psi_4'(L) = \psi_4(L) = 0\ . \end{aligned} \tag{2.9}$$

Consequently

$$\begin{aligned} \psi_1 &= 1 - 3(x/L)^2 + 2(x/L)^3 \\ \psi_2 &= x - 2L(x/L)^2 + L(x/L)^3 \\ \psi_3 &= 3(x/L)^2 - 2(x/L)^3 \end{aligned} \tag{2.10}$$

and $\psi_4 = -L(x/L)^2 + L(x/L)^3$.

It follows from the energy relations (2.3a) and (2.4) that

$$k_{ij} = \int_0^L EI(x)\psi_i''\psi_j''\,dx \tag{2.11}$$

$$m_{ij} = \int_0^L m\,\psi_i\,\psi_j\,dx \tag{2.12}$$

where I(x) is given in equation(2.2d).

The resulting analytical expressions for [K] and [M] are fairly straightforward. Elements of the four-by-four symmetric stiffness matrix are given by the following expressions.

$$\begin{aligned} k_{11} = -k_{13} = k_{33} &= \frac{12EI_0}{L^3}\left[1 + \frac{2}{5}(\beta L)^2 - (\beta L)\right] \\ -k_{12} = k_{23} &= \frac{6EI_0}{L^2}\left[1 + \frac{7}{30}(\beta L)^2 - 2(\beta L)\right] \\ k_{14} = -k_{34} &= \frac{6EI_0}{L^2}\left[1 + \frac{17}{30}(\beta L)^2 - \frac{4}{3}(\beta L)\right] \end{aligned} \tag{2.13}$$

$$k_{22} = \frac{4EI_0}{L}\left[1 + \frac{2}{15}(\beta L)^2 - \frac{1}{2}(\beta L)\right]$$

$$k_{24} = \frac{2EI_0}{L}\left[1 + \frac{13}{30}(\beta L)^2 - (\beta L)\right]$$

and

$$k_{44} = \frac{4EI_0}{L}\left[1 + \frac{19}{30}(\beta L)^2 - \frac{3}{2}(\beta L)\right].$$

Although the deflected shape of the beam, $v(x)$, is not a function of βL, the stiffness coefficient k_{ij} are polynomials of βL, because the flexural rigidity, EI, depends upon βL. The case of a uniform beam is obtained by substituting $\beta L = 0$ into the above stiffness equations. The conventional stiffness coefficients are then obtained.

However, the mass matrix is independent of βL because m_0 is a constant. Equation (2.12) yields the consistent mass matrix for a uniform beam element which can be found in reference [8].

In contrast, analytical expressions for the stiffness and mass matrices become very complicated when the alternative relation (2.6) is used. Nevertheless, the numerical evaluation of k_{ij} and m_{ij} can be accomplished as follows. Firstly, apply the boundary conditions to relation (2.6), so that

$$\begin{Bmatrix} v_1 \\ v_2 \\ v_3 \\ v_4 \end{Bmatrix} = \begin{bmatrix} 0 & 0 & 1 & 1 \\ \beta & -\beta & -\beta & 0 \\ -\mathrm{Ln}(1-\beta L) & (1-\beta L)\mathrm{Ln}(1-\beta L) & (1-\beta L) & 1 \\ \beta/(1-\beta L) & -\beta(1+\mathrm{Ln}(1-\beta L)) & -\beta & 0 \end{bmatrix} \begin{Bmatrix} C_1 \\ C_2 \\ C_3 \\ C_4 \end{Bmatrix} \tag{2.14a}$$

or $\{V\} = [\, D_1 \,] \{C\}$. (2.14b)

The matrix $[\, D_1 \,]$ is evaluated for a particular element and is inverted in order to obtain

$$\{C\} = [\, D \,] \{V\} \tag{2.15}$$

in which $[\, D \,]$ equals $[\, D_1 \,]^{-1}$. Now from the energy relation (2.3) and equation (2.6)

$$\sum_{i=1}^{4} \sum_{j=1}^{4} k_{ij}\, v_i\, v_j = \frac{1}{2} \int_0^L EI (v'')^2 \, dx \tag{2.16}$$

$$\sum_{i=1}^{4} \sum_{j=1}^{4} k_{ij}\, v_i\, v_j = \frac{1}{2}\, EI\, \beta^3 L \left[C_2^2 \beta L + C_1^2 \frac{\beta L}{1-\beta L} + 2C_1 C_2\, \mathrm{Ln}(1-\beta L)\right]. \tag{2.17}$$

Similarly, by using energy relation (2.4) and equation (2.7)

$$\sum_{i=1}^{4} \sum_{j=1}^{4} m_{ij} v_i\, v_j = \frac{1}{2}\, m \int_0^L (v(x))^2 \, dx \tag{2.18a}$$

$$\sum_{i=1}^{4} \sum_{j=1}^{4} m_{ij} v_i\, v_j = \frac{1}{2}\, m \int_0^L \{C_1 \mathrm{Ln}(1-\beta x) + C_2(1-\beta x)\, \mathrm{Ln}(1-\beta x) + C_3(1-\beta x) + C_4\}^2 \, dx . \tag{2.18b}$$

For fixed values of i and j (i,j = 1 to 4) the elements of the symmetric stiffness and mass matrices can be evaluated by substituting the numerical values for $C_k C_m$ in Equations (2.17) and (2.18b) as

$$C_k C_m = \sum_{i=1}^{4} \sum_{j=1}^{4} D_{ki}\, D_{mj}\, v_i\, v_j \qquad (k,m = 1 \text{ to } 4). \tag{2.19}$$

A restriction of this method is that the logarithmic function βL cannot take a value of zero or unity. Hence, these two values may be approximated as 0.01 or 0.99, respectively. Further in the chapter this approximation will be justified pertaining to results shown in Table I(a) and (b).

Natural frequency computations were carried out for a cantilever beam. Results from the two different finite element approximations, based on Equations (2.6) and (2.7), were compared with analytical frequencies.

Properties of the uniform and tapered test beams are as shown in Figure 2.3.

The analytical expression for the natural frequencies of a uniform cantilever beam is given as [3]

$$\omega_n = C_n \sqrt{\frac{EI}{mL^4}} \text{ Hz.} \tag{2.20}$$

in which n=1,2,3,... and $C_1 = 0.560, C_2 = 3.51, C_3 = 9.82$. Also the analytical expression for a tapered cantilever beam, derived in reference [7], are the roots of

$$J_0(\tau\sqrt{L})\, I_1(\tau\sqrt{L}) + I(\tau\sqrt{L})\, J_1(\tau\sqrt{L}) = 0 \tag{2.21}$$

where $\tau = 2(m\,\omega^2\,L^2/EI)^{1/4}$ and I_n and J_n, respectively, are modified and ordinary Bessel functions of the nth order and first kind.

Table I(a) shows the comparison of natural frequencies for a straight cantilever beam, obtained analytically and by

using the finite element method with either the simple cubic polynomial given by Equation (2.7) and/or the logarithmic expression from equation (2.6) as mode shapes. Table I(b) shows the comparison for the tapered cantilever beams. Table I(c) shows the comparison of the fundamental frequencies for

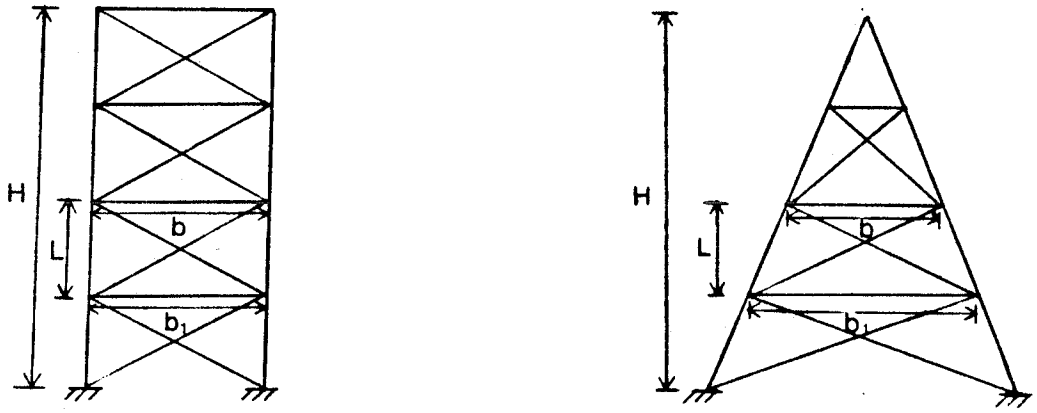

(a) (b)

Figure 2.3: Typical (a) straight and (b) tapering sections.

Straight beam	Tapered beam
H = 30.48 m	H = 4 m
A = 0.0062 m^2	A = 1 m^2
B1 = B = 6.706 m	B1 = 1 m
E = 0.2048 $X10^8 N/m^2$	E = 1 N/m^2
m = 421 Kg/m	m = 1 Kg/m
L = 7.62 m	L = 1 m
Number of elements = 4	Number of elements = 4

tapered beams with varying aspect ratio bL.

Results in Table I(a) show that, for the uniform beam ($\beta L = 0$) shown in Figure 2.3(a), a cubic polynomial method gave frequencies which are comparable with analytical results.

TABLE I

(a) Comparison of natural frequencies for the straight beam
Aspect ratio $\beta L = 0$

Mode	Natural Frequency in rad/sec		
	Finite Element Method		Analytical Results
	Cubic Polynomial	Logarithmic Expression*	
1	0.440	0.426	0.440
2	2.760	2.670	2.757
3	7.779	7.520	7.715
4	15.340	14.819	15.085

* Using $\beta L \simeq 0.01$

(b) Comparison of natural frequencies for the tapered beam
Aspect ratio $\beta L = 1.0$

Mode	Natural Frequency in rad/sec		
	Finite Element Method		Analytical Results
	Cubic Polynomial	Logarithmic Expression**	
1	8.164	2.576	2.553
2	14.699	10.307	9.942
3	21.782	23.692	22.276
4	42.778	48.452	39.546

** Using $\beta L \simeq 0.99$

(c) Comparison of fundamental frequency for the tapered beam Aspect ratio between zero and unity.

βL	fundamental Frequency in rad/sec		
	Finite Element Method		Analytical Results***
	Cubic Polynomial	Logarithmic Expression	
0.9	7.949	2.711	2.628
0.8	7.560	2.835	2.762

*** These reults were obtained by using Dunkerley's method [7]. They are 2 to 4% lower than the corresponding exact results.

Conversely, it can be seen from Table I(b) that the analogous natural frequencies for a tapered beam ($\beta L = 1.0$), shown in Figure 2.3(b), have enormous discrepancies. However, the logarithmic expression gave reasonably good results for both a straight beam (using $\beta L \simeq 0.01$) and for a tapered beam (using $\beta L \simeq 0.99$). Results in Table I(c) also show the suitability of the logarithmic expression for aspect ratios, between zero and one. Therefore, it is clear that, in case of the straight beam, both the cubic polynomial and the logarithmic expression can be employed for the generation of the stiffness and mass matrices. However, the cubic polynomial is simpler and computationally more efficient than the logarithmic expression, so that the former is best suited for nearly straight beam. On the other hand, the logarithmic expression is preferred to the cubic polynomial for tapered beams.

A typical tower such as that shown in Figure 1.1 has both straight and tapered beam segments. Therefore, a computer package was developed to have two options. A cubic polynomial was employed for uniform segments whereas a logarithmic expression was used for tapered segments

2.2.2 Torsion

A lattice segment derives almost all its torsional rigidity from the bracing elements which interconnect the main legs of a tower. The torsional rigidity of a lattice member changes with the type of bracing used. Consider, for example, a typical tapering lattice beam with the most commonly used X-shaped bracing members. Each bracing member is supposed to have the cross-sectional area A_b as shown in Figure 2.4.

The expression for the torsional rigidity of such a cell can be approximated as [7]

$$GJ = 2\sqrt{2}\,\frac{E\,A\,b_1^2}{(b_1+b)^2}\,b \qquad (2.22)$$

where A_b is the area of the bracing.

Similar expressions may be developed for other types of bracing, such as for K-shaped bracing [7].

The mass per unit length, m, of the segment may be separated into the leg mass, m_L, located at the corners of a cross-section, and a bracing mass, m_b, distributed approxi-

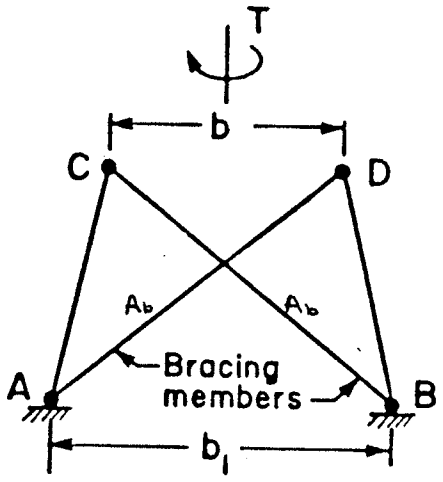

Figure 2.4: Typical X-bracing cell

mately uniformly along the sides. A reasonable approximation for the torsional inertia per unit length is [7]

$$m_r = (m_L/2 + m_b/3)\, b^2 \text{ or } m_r = m_0 (1 - \beta x)^2 \qquad (2.23a)$$

where b is the width of a segment at any section X-X and

$$m_0 = (m_L/2 + m_b/3) b_1^2 . \qquad (2.23b)$$

The equilibrium equation for an element loaded statically by an end torque is given as [8]

$$(GJ\, \theta')' = 0 . \qquad (2.24)$$

Let the assumed mode shape, which satisfies boundary conditions as well as the equilibrium equation, be given as

$$\psi_1 = 1 - x/L \quad \text{and} \quad \psi_2 = x/L . \qquad (2.25)$$

A similar procedure to that adopted in section 2.2.1 is used to obtain the torsional stiffness and mass matrices which are given in Appendix B. However, it is the mass matrix which differs from that of a uniform beam in this case, because the torsional inertia depends upon βL.

2.2.3 Axial

As mentioned earlier in section 2.2.1, the area of a supporting leg remains constant along its length. Therefore, the tapered lattice segment can be modelled as a uniform beam for the case of axial deformation. The stiffness and mass matrices for the axial motion of a uniform beam can be found in reference [8] and are given, for completeness, in Appendix B.

2.2.4 Geometric stiffness matrices

The effect of an axial load and self weight on the bending stiffness of a beam element were not considered in section 2.2.1. However, the axial load on an element and its own self weight are quite significant practically [9]. Hence, the elemental stiffness matrix should be modified for these kind of loads.

In the case of a cubic polynomial approximation, the geometric stiffness matrix for the axial load is given as

$$K_{GA_{ij}} = \int_0^L P\ \psi_i'\ \psi_j'\ dx \qquad (2.26)$$

and the geometric stiffness matrix for the self weight of the member is found from

$$K_{GW_{ij}} = \int_0^L q_0\ x\ \psi_i'\ \psi_j'\ dx\ . \qquad (2.27)$$

Here ψ_i and ψ_j are as given in equation (2.10), P is the compressive axial force on the member and q_0 is the self weight per unit length of the member.

In the case of the logarithmic expression, however, it can be seen that

$$K_{GAij} = \int_0^L P\,(v')^2\,dx \qquad (2.28)$$

and $$K_{GUij} = \int_0^L q_0\,x\,(v')^2\,dx \qquad (2.29)$$

where v'(x) is given by equation (2.6) and C_1 through C_4 may be obtained from equation (2.19).

Finally, the modified stiffness is given as

$$K \text{ modified} = k_{ij} + K_{GAij} + K_{GUij} \qquad (2.30)$$

in which k_{ij} is given by equation (2.11) or (2.16), depending upon the approximation chosen.

2.3 Practical implementation of the finite element modelling.

The transmission tower shown in Figure 2.5a was analysed to assess the accuracy of the finite element modelling. The tower was idealized as shown in Figure 2.5b . An assembly of nine segments was employed with each segment being treated as a beam element having six degrees of freedom per node.

The lowest natural frequencies for the same tower are available from a SAPIV finite element model which employed 452 beam and 176 truss elements [10]. Table II compares the natural frequencies for in-plane bending, out-of-plane bending and torsion. It can be seen that the results obtained by using the algorithm detailed in this chapter are comparable to those obtained from SAPIV [10] but gives an overestimate of the natural frequencies. The probable reason for this is

the use of consistent mass matrix in the present algorithm, whereas, SAPIV employs a lumped mass matrix. Another probable reason is the approximate idealization of the lattice segment in form of a beam element, which could give an overestimate of the stiffness.

TABLE II Comparison of the Fundamental natural frequencies of the transmission tower of Figure 2.5.

Mode Shapes	Fundamental Natural Frqeuencies Hz	
	Present model	SAPIV model
In-plane Bending	4.02	3.92
Out-of-plane Bending	4.39	3.97
Torsion	6.52	6.19

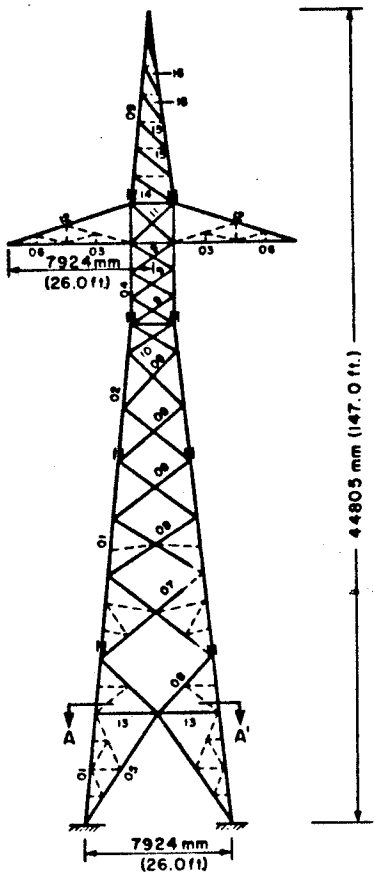

TRANSVERSE ELEVATION
(LONGITUDINAL ELEVATION SIMILAR)

(a) Structural Details

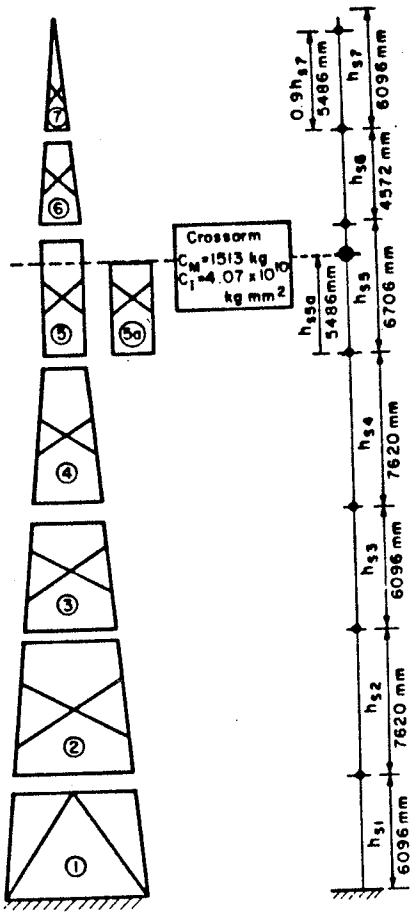

Segments

(b) Idealization

Member	Size of Angle (mm)	Cross Section (mm)^2
01	203x203x15.9	6200
02	203x203x12.7	5000
03	152.5x152.5x11.1	3264
04	152.5x152.5x12.7	3710
05	152.5x101.5x7.9	1955
06	127x127x9.5	2329
07	102x102x7.9	1548
08	102x102x6.4	1252
09	89x 89x6.4	1090
10	76x 76x6.4	929
11	76x 76x4.8	703
12	76x 63.5x6.4	845
13	76x 63.5x4.8	645
14	63.5x63.5x4.8	581
15	51x 51x4.8	458
16	44.5 x 44.5x4.8	400

Segment (i)	m kg/mm	A_L mm^2	A_b mm^2	H_t mm	b_1 mm
1	0.435	6200	1955	39 624	7925
2	0.421	6200	1252	33 528	6706
3	0.381	6200	1252	25 908	3962
4	0.299	5000	1252	19 812	3962
5,5a	0.267	3710	1090		2438
6	0.081	1090	229	10 668	2438
7	0.052	1090	229	6096	1394

Figure 2.5: Typical Transmission Tower

Chapter III

CABLE STRUCTURE

3.1 Introduction

A cable hanging under its own weight generally follows a catenary profile [13]. However, for the case of a structural guy which supports a tower, the pretension is high and the sag is very small. In this situation, the catenary profile can be approximated by a parabola. This approximation, which is reasonable for sag-to-span ratios of 1/8 or less, greatly simplifies an analysis.

Various authors [4,13,14] have produced convenient linearized approximations to the equation of motion of a cable hanging in a parabolic profile. Irvine has given expressions for the natural frequencies of a horizontal cable fixed at both ends and oscillating in-plane and out-of-plane. These expressions are functions of several parameters such as the axial rigidity $A_c E_c$, pre-tension in the cable, T_0, the self weight per unit of chord length, q_y, and the span length of the cable, L_c. Veletsos [4] has considered the inclined cable shown in Figure 3.1. This cable is fixed at the base and free to move at the upper end, which is presumed to be attached to a tower as shown in Figure 3.2a. Veletsos present-

ed expressions for the dynamic stiffness at the upper, moveable end of the cable which correspond to the displacements in three directions. These expressions are functions of frequency and they can be added to the stiffness matrix of the tower itself to produce a set of transcendental equations

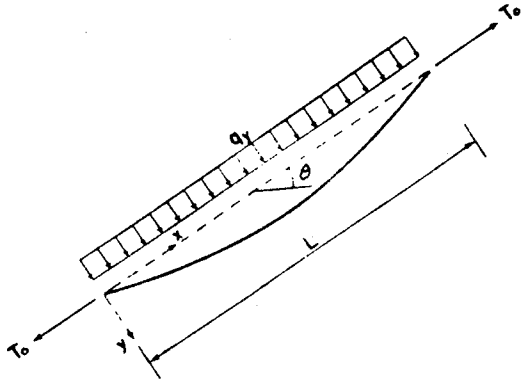

Figure 3.1: Typical inclined cable

for the natural frequencies, ω_n. A solution to these equations can be obtained by using an incremental search method. However, because the cable stiffness, $K(\omega)$, is a discontinuous function, there is a chance of missing a particular ω_n. It is more reliable to solve a standard eigenvalue problem. Therefore, a finite element representation of a parabolic cable will be developed in this chapter. The accuracy of the finite element technique will be verified by comparison with the analytical results for a horizontal cable.

3.2 Finite element method

The finite element approach may be formulated for an inclined cable by considering the typical element shown in Figure 3.2b. Let u, v, and w be the end displacements of the cable element along the positive x, y, and z directions, respectively, so that there are generally six degrees of freedom. The force-displacement relation is

$$\{P\} = [S]\ \{W\} \tag{3.1}$$

where $\{W\}$ is composed of the elements $< u_1\ v_1\ w_1\ u_2\ v_2\ w_2 >^T$, $\{P\}$ is the load vector and $[S]$ is the stiffness matrix derived in Appendix C. Matrix $[S]$ has the form

$$[S] = \begin{bmatrix} K_{xx} & K_{xy} & 0 & -K_{xx} & -K_{xy} & 0 \\ & K_{xy} & 0 & -K_{xy} & -K_{yy} & 0 \\ & & K_{zz} & 0 & 0 & -K_{zz} \\ & & & K_{xy} & -K_{yy} & 0 \\ & \text{Symmetric} & & & K_{yy} & 0 \\ & & & & & K_{zz} \end{bmatrix}. \tag{3.2}$$

It can be seen from relation (3.2) that there are only four different stiffness coefficients K_{xx}, K_{xy}, K_{yy} and K_{zz}. These coefficients can be expressed conveniently in terms of the local coordinate system of the cable. Inertias corresponding to each degree of freedom are lumped at each node of the element. This procedure results in a six-by-six diagonal mass matrix for the cable. In special situations, where only in-plane vibrations are excited, the out-of-plane de-

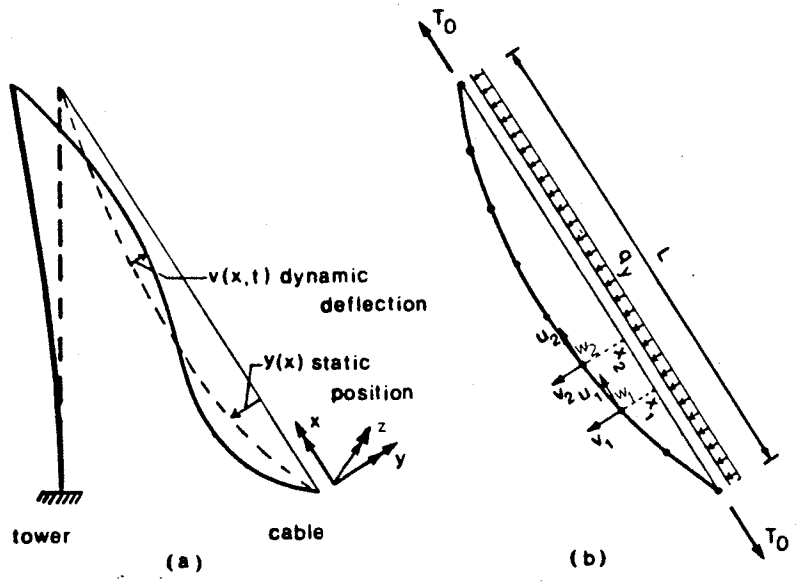

Figure 3.2 Modelling of the vibration of an inclined cable
(a) Theoretical dynamic configuration, and
(b) representation by parabolic cable element with degrees of freedom u, v, and w given in local coordinates

grees of freedom may be treated as dummy degrees of freedom. Then only the four by four stiffness and mass matrices need be assembled. This simplification greatly reduces the size of the resulting eigenvalue problem and, hence, the computational effort.

When the transverse dynamic displacement is combined with a quasi-static axial stretching of the cable, the inertia forces can be assumed to act only in the transverse direction. This assumption is reasonable for the lower-frequency transverse modes because the wavelength of axial vibration is then very much greater than the length of cable [14].

The accuracy of the finite element model may be assessed by a comparison with analytical results. However, analytical results are available for only a few cases. For instance, in the case of a horizontal cable like that shown in Figure 3.3, the transverse natural frequencies are given by Irvine [13]. A distinction must be made in the analytical solution between the symmetric modes, which have an odd number of vibration loops per span, and the anti-symmetric modes which have an even number. The characteristic equation for the symmetric modes is [13]

$$\tan(\omega_{ns}) = \omega_{ns} - \frac{4}{\lambda^2}(\omega_{ns})^3 \qquad (3.3)$$

$$\text{where} \quad \omega_{ns} = \omega_s L \,/\, (T_0/m)^{1/2} \qquad (3.4)$$

and ω_s is the natural frequency of the symmetric in-plane mode. The ω_{ns} is the normalized value of ω_s and m is the mass per unit length of the cable. Also, λ^2 is a factor depending upon the flexibility of the cable. It is given by

$$\lambda^2 = \left(\frac{q_y L_c}{T_0}\right)^2 L_c \Big/ \left(\frac{T_0 L_e}{A_c E_c}\right) \qquad (3.5)$$

where L_e is an effective length as given by Equation (C5). The case $\lambda^2=0$ represents a perfectly flexible cable and $\lambda^2=\infty$ represents a rigid cable. For a guyed-tower structure, λ^2 ranges typically between 2 and 60. Solutions giving ω_{ns} for various values of λ^2 are available in [13].

In contrast, the natural frequencies of the anti-symmetric in-plane modes are independent of the flexibility and they are given by

$$\omega_a = 2n\pi \left(\frac{T_0}{m}\right)^{1/2}, \text{ where } n=1,2,3..... \qquad (3.6)$$

These frequencies happen to be the anti-symmetric modal frequencies of a taut wire. Similarly, the natural frequencies for out-of-plane vibrations are independent of the flexibility and are given by the taut wire relation

$$\omega_o = n\pi\left(\frac{T_o}{m}\right)^{1/2} \quad , \text{ where } n=1,2,3.... \quad . \qquad (3.7)$$

This last relation encompasses both the symmetric and anti-symmetric modes. The reasonableness of the expressions for natural frequencies in all three modes has been confirmed

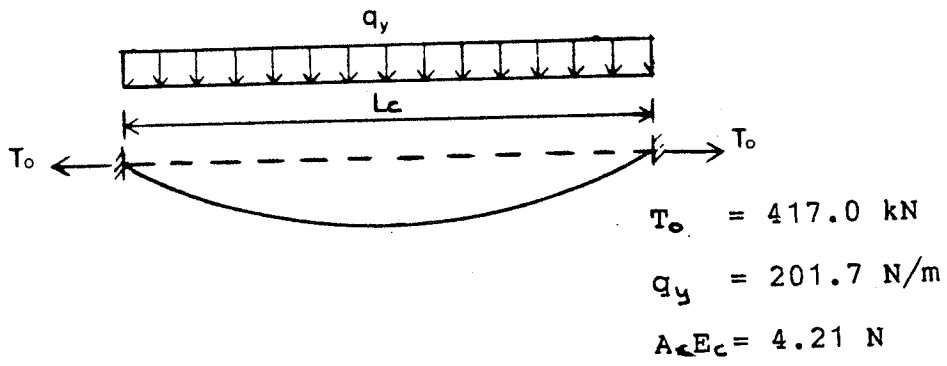

Figure 3.3: Typical test cable

experimentally in reference [15].

The horizontal cable shown in Figure 3.3 will now be studied using the finite element analysis. Both the in-plane and out-of-plane natural frequencies will be determined and compared with theoretical results described above. Also, the effect of the flexibility coefficient, λ^2, on the natural frequencies will be studied. Values of λ^2 between 2 and 60 typically represent the range of situations for structural guys. Such a variation can be obtained most conveniently

by changing the cable length, L_c, in expression (3.5). In other words, the values of L_c which were chosen in this example are essentially dummy variables. Although they range from 92 to 500 metres, they are not intended to represent the typical length of a guy or conductor cable.

Tables III(a) and (b) present results for the in-plane natural frequencies. It can be seen that an idealization of eight elements produces reasonable accuracy for the first four transverse natural frequencies (two symmetric and two antisymmetric). The error increases from only 1.7% for the first symmetric mode to 10.0% for the second antisymmetric mode. Similarly, sixteen elements produce reasonable accuracy for the first eight transverse natural frequencies. Results for the out-of-plane natural frequencies shown in Table III(c) give the same trends. In all cases, there is no significant variation in error magnitude with the flexibility parameter, λ^2, at least in the range of interest for guyed towers. Also, only the first few transverse modes are required, so that the longitudinal motions can be considered quasi-static. This last contention was verified by comparing results obtained with and without longitudinal inertia. There was no difference in results at all.

Condensation techniques can sometimes reduce computational effort whilst maintaining accuracy. In the present example, degrees of freedom were condensed by using a technique known as Guyan's reduction [8] at alternate nodes. This pro-

cedure halves the size of the eigenvalue problem for a given number of elements. Results for in-plane symmetric vibrations are shown in Table IV. They may be compared with the results shown in Table III(a). It can be seen that Guyan's reduction technique is significantly less accurate for a given number of elements. Further, the use of 17 elements with Guyan's reduction gives comparable accuracy to a straightforward technique with only 8 elements. This finding supports the contention that Guyan's reduction technique is not successful when a lumped mass matrix is used [8].

Table III(a) In-Plane symmetric mode

Number of Elements = 8 CPU Time = 1.06 sec

λ^2	Length (m)	Normalized natural frequencies rad/sec			
		Mode	FEM results	Analytical results	% Error
60	506.3	ω_1/π	2.32	2.29	1.3
		ω_2/π	2.97	3.18	6.6
		ω_3/π	4.24	5.03	15.7
		ω_4/π	4.99	7.01	28.8
20	291.6	ω_1/π	1.58	1.61	1.7
		ω_2/π	2.86	3.04	6.0
		ω_3/π	4.24	5.01	15.5
		ω_4/π	5.00	7.00	28.6
6	159.6	ω_1/π	1.21	1.22	1.0
		ω_2/π	2.83	3.01	5.9
		ω_3/π	4.24	5.00	15.3
		ω_4/π	5.00	7.00	28.6
2	92.1	ω_1/π	1.07	1.08	0.8
		ω_2/π	2.83	3.01	5.9
		ω_3/π	4.24	5.00	15.3
		ω_4/π	5.00	7.00	28.6

(Contd.)

(Contd.)

Number of Elements = 16 CPU Time = 7.0 sec

λ^2	Length (m)	Normalized natural frequencies rad/sec			
		Mode	FEM results	Analytical results	% Error
60	506.3	ω_1/π	2.27	2.29	0.9
		ω_2/π	3.12	3.18	1.9
		ω_3/π	4.81	5.03	4.4
		ω_4/π	6.45	7.01	8.0
20	291.6	ω_1/π	1.60	1.61	0.5
		ω_2/π	2.99	3.04	1.7
		ω_3/π	4.80	5.01	4.1
		ω_4/π	6.46	7.00	7.7
6	159.6	ω_1/π	1.22	1.22	0.2
		ω_2/π	2.97	3.01	1.5
		ω_3/π	4.80	5.00	4.0
		ω_4/π	6.46	7.00	7.7
2	92.1	ω_1/π	1.08	1.08	0.3
		ω_2/π	2.96	3.01	1.7
		ω_3/π	4.80	5.00	4.0
		ω_4/π	6.46	7.00	7.7

Table III(b) In-Plane anti-symmetric mode

Number of Elements = 8 CPU Time = 1.06 sec

λ^2	Length (m)	Normalized natural frequencies rad/sec			
		Mode	FEM results	Analytical results	% Error
60	506.3	ω_1/π	1.94	2.00	3.1
		ω_2/π	3.59	4.00	10.3
		ω_3/π	4.70	6.00	21.8
		ω_4/π	**	**	**
20	291.6	ω_1/π	1.95	2.00	2.7
		ω_2/π	3.60	4.00	10.1
		ω_3/π	4.70	6.00	21.6
		ω_4/π	**	**	**
6	159.6	ω_1/π	1.95	2.00	2.6
		ω_2/π	3.60	4.00	10.0
		ω_3/π	4.70	6.00	21.6
		ω_4/π	**	**	**
2	92.1	ω_1/π	1.95	2.00	2.5
		ω_2/π	3.60	4.00	10.0
		ω_3/π	4.70	6.00	21.6
		ω_4/π	**	**	**

(Contd.)

(Contd.)

Number of Elements = 16 CPU Time = 7.0 sec

λ^2	Length (m)	Normalized natural frequencies rad/sec			
		Mode	FEM results	Analytical results	% Error
60	506.3	ω_1/π	1.97	2.00	1.3
		ω_2/π	3.88	4.00	3.0
		ω_3/π	5.64	6.00	6.0
		ω_4/π	7.18	8.00	10.3
20	291.6	ω_1/π	1.98	2.00	0.9
		ω_2/π	3.89	4.00	2.7
		ω_3/π	5.65	6.00	5.8
		ω_4/π	7.20	8.00	10.0
6	159.6	ω_1/π	1.99	2.00	0.7
		ω_2/π	3.90	4.00	2.6
		ω_3/π	5.66	6.00	5.7
		ω_4/π	7.20	8.00	10.0
2	92.1	ω_1/π	1.99	2.00	0.7
		ω_2/π	3.90	4.00	2.6
		ω_3/π	5.66	6.00	5.7
		ω_4/π	7.20	8.00	10.0

Table III(c) Out-of-Plane mode

Number of Elements = 8 CPU Time = 1.06 sec

λ^2	Length (m)	Normalized natural frequencies rad/sec			
		Mode	FEM results	Analytical results	% Error
60	506.3	ω_1/π	0.99	1.00	0.6
		ω_2/π	1.95	2.00	2.6
		ω_3/π	2.83	3.00	5.7
		ω_4/π	3.60	4.00	10.0
20	291.6	ω_1/π	0.99	1.00	0.6
		ω_2/π	1.95	2.00	2.6
		ω_3/π	2.83	3.00	5.7
		ω_4/π	3.60	4.00	10.0
6	159.6	ω_1/π	0.99	1.00	0.6
		ω_2/π	1.95	2.00	2.6
		ω_3/π	2.83	3.00	5.7
		ω_4/π	3.60	4.00	10.0
2	92.1	ω_1/π	0.99	1.00	0.6
		ω_2/π	1.95	2.00	2.6
		ω_3/π	2.83	3.00	5.7
		ω_4/π	3.60	4.00	10.0

(Contd.)

(Contd.)

Number of Elements = 16 CPU Time = 7.0 sec

λ^2	Length (m)	Normalized natural frequencies rad/sec			
		Mode	FEM results	Analytical results	% Error
60	506.3	ω_1/π	1.00	1.00	0.2
		ω_2/π	1.99	2.00	0.7
		ω_3/π	2.96	3.00	1.4
		ω_4/π	3.90	4.00	2.5
20	291.6	ω_1/π	1.00	1.00	0.2
		ω_2/π	1.99	2.00	0.7
		ω_3/π	2.96	3.00	1.4
		ω_4/π	3.90	4.00	2.5
6	159.6	ω_1/π	1.00	1.00	0.2
		ω_2/π	1.99	2.00	0.7
		ω_3/π	2.96	3.00	1.4
		ω_4/π	3.90	4.00	2.5
2	92.1	ω_1/π	1.00	1.00	0.2
		ω_2/π	1.99	2.00	0.7
		ω_3/π	2.96	3.00	1.4
		ω_4/π	3.90	4.00	2.5

Table IV Guyan's reduction technique

Number of Elements = 9

λ^2	Length (m)	Normalized natural frequencies rad/sec			
		Mode	FEM results	Analytical results	% Error
60	506.3	ω_1/π	2.07	2.29	9.6
		ω_2/π	2.83	3.18	11.1
20	291.6	ω_1/π	1.53	1.61	5.0
		ω_2/π	2.50	3.04	7.7
6	159.6	ω_1/π	1.18	1.22	3.0
		ω_2/π	2.49	3.01	17.4
2	92.1	ω_1/π	1.05	1.08	2.5
		ω_2/π	2.48	3.01	17.3

(Contd.)

(Contd.)

Number of Elements = 17

λ^2	Length (m)	Normalized natural frequencies rad/sec			
		Mode	FEM results	Analytical results	% Error
60	506.3	ω_1/π	2.22	2.29	2.9
		ω_2/π	3.01	3.18	5.5
		ω_3/π	4.33	5.03	13.8
		ω_4/π	5.21	7.01	25.7
20	291.6	ω_1/π	1.59	1.61	1.5
		ω_2/π	2.88	3.04	5.2
		ω_3/π	4.32	5.01	13.7
		ω_4/π	5.21	7.00	25.6
6	159.6	ω_1/π	1.21	1.22	0.9
		ω_2/π	2.86	3.01	5.1
		ω_3/π	4.32	5.00	13.6
		ω_4/π	5.21	7.00	25.6
2	92.1	ω_1/π	1.07	1.08	0.8
		ω_2/π	2.85	3.01	5.0
		ω_3/π	4.32	5.00	13.6
		ω_4/π	5.20	7.00	25.6

Chapter IV

DYNAMICS OF A GUYED TRANSMISSION TOWER SYSTEM.

The contents of this chapter are related to the free vibration analysis of the tower system shown in Figure 4.1. The analysis is based on the finite element models for tower and cable developed in Chapters II and III, respectively. For completeness certain sections from previous chapters reappear in this chapter.

4.1 Introduction

The guyed tower shown in Figure 4.2 has been designed by Manitoba Hydro as the tangent suspension structure for their 138 kV Radisson-Churchill transmission line. The Y-shaped frame is pinned at the base and consists of high-strength steel sections which are bolted together. The concept should allow a more rapid erection of the line as compared to a standard lattice design, and is especially cost-beneficial in the remote northern terrain. The tower is also less obtrusive visually, especially since the structure will have the dark rust finish of natural weathering steel.

A structural analysis has been based primarily on static considerations as is usual in current practice. However, the transmission line passes

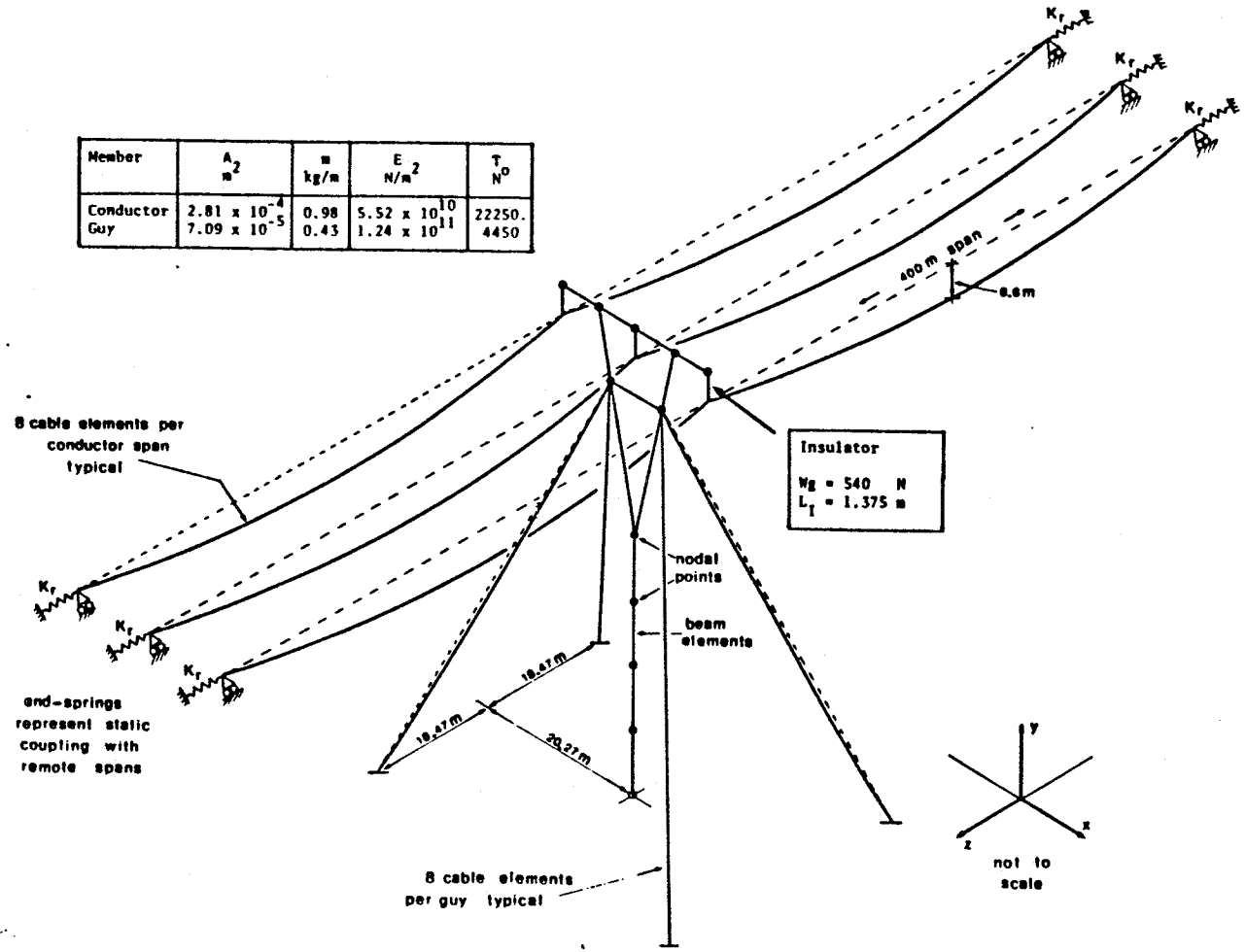

Figure 4.1: Finite Element Model of the Tower and Transmission Line

through a region close to Hudson's Bay where frequent icing is possible. Therefore, large-amplitude conductor vibration known as galloping may develop. Also, the design for a radial ice load of 44 mm indicates that there may be large transient longitudinal loads due to sudden shedding of ice. There was concern that such dynamic loads might be critical because the structure does not carry groundwires.[1] In a standard design, these wires would normally provide a restraint, limiting the bending or torsional stress in the tower caused by longitudinal loads [16,17]. Also, a key structural feature is the welded box connection shown in detail A of Figure 4.2. This box is designed to develop the full static strength of the adjacent 200x200-mm members and the 275-mm diameter stem. However, it is necessary to ensure that there are not excessive flexural or torsional vibrations at this location; otherwise fatigue of the welded joints may develop.

This chapter outlines the results of an analysis of the free-vibration characteristics of the transmission-line system. Such a study gives the relative modal displacements for each of the different components: tower, guys, insulators and conductors. It is then possible to assume a galloping amplitude and, hence, compute the displacements and stresses in the tower's structural components [18]. There is some question as to the accuracy of a linear vibration analysis

[1] Groundwires were not used because the structures were located at a low isokeraunic level.

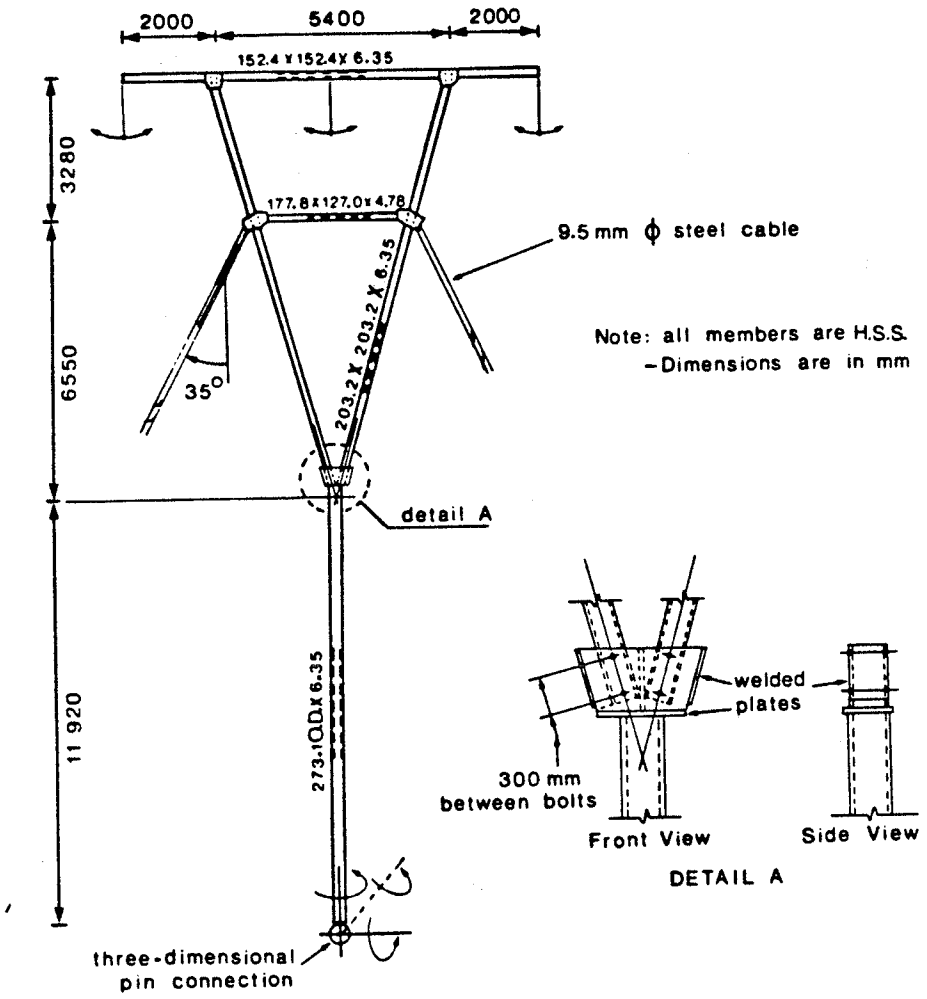

Figure 4.2: Structural Details of the Y-tower.

because galloping amplitudes are large. However, even 6 metres of galloping is small in comparison to a span of 400 metres. Further, it was argued in reference [18] that theoretical estimates of the lowest natural frequencies of a conductor are close to those determined from experimental records of large-amplitude galloping.

4.2 Theoretical modelling

The dynamic analysis of a transmission tower structure is complicated because there are a number of components which may interact. These are (1) the structural steel frame, (2) the inclined guy-wires, (3) the insulator strings, and (4) the conductors.

Each component is distinctly different and, if interactions are indeed important, a finite element approach is also mandatory. Specialized types of elements are used to model the dynamic bending of the tower's frame, elongation and transverse displacement of conductors and guys (in the plane of the sag) and the rigid-body rotations of insulators. Details of the application and theory of the modelling will be discussed only briefly here since appropriate references are given.

4.2.1 Tower's Frame

The steel Y-frame was modelled using thirteen beam elements having stiffness in both bending and torsion. There are twelve nodal points as shown Figure 4.1. A complication arises from the fact that the tower carries significant compressive load due to its self weight, the conductors' weight and the prestress in the four guys. Such loads are likely to reduce the bending stiffness of the structure and, therefore, lower the natural frequencies. They were incorporated

into the finite element model by means of a geometric stiffness matrix [8].

4.2.2 Inclined guy wires

Previous dynamic analyses of guyed transmission towers have been performed by Tsui [18] and by Kempner et al [19]. However, in reference [18] the guys were represented simplistically by a single axial element. No attempt was made to simulate transverse vibration in a guy. On the other hand, transverse vibrations were considered in reference [8] using 10 straight beam elements to approximate the cable's profile. Arbitrary, but small, values of torsional and flexural rigidity could be then specified to stabilize the movement of interior nodes. Also, the cable's static pretension, T_0, which is a crucial parameter, was accommodated by employing a geometric stiffness matrix. However, although this model appears reasonable, a beam element requires twelve degrees of freedom and hence computational effort can be onerous.

An alternative approach utilizing specialized parabolic cable elements has been developed. Such elements can represent more accurately the cable profile and yet each has only four degrees of freedom. The element's characteristics are derived from the linearized theory of cable dynamics summarized in references [13,14]. In particular, the cable modelling is intended to approximate reasonably the accurate

theoretical work of Veletsos and Darbre [4]. They studied the situation of an inclined vibrating guy interacting with the tower illustrated in Figure 3.2a. The ensuing finite element shown in Figure 3.2b has an axial degree of freedom, u, parallel to the x or chord axis, and a transverse degree of freedom, v, perpendicular to the chord. The four-by-four symmetric stiffness matrix for an element is derived in terms of the local coordinates x_1 and x_2 and is listed in Chapter III. Corresponding inertias are lumped at each end of the element but the inertia forces are assumed to act only in the transverse direction. In other words, the transverse dynamic displacement v is combined with a quasi-static axial stretching of the entire cable. This assumption [4,14] is reasonable for the lower-frequency modes because the wavelength of axial vibrations is then very much greater than the length of cable.

The stiffness and mass matrices may easily be extended to six by six to include out-of-plane motions of the guys. Stiffnesses for motion in the local z-direction, where x, y and z is a right-handed coordinate system, are also given in Chapter III. The importance of out-of-plane guy motions will be studied.

4.2.3 Insulator strings

The insulator shown in Figure 4.3 is subjected to a horizontal force P_A at the crossarm level. Therefore, it undergoes a rigid body displacement. The translation, U_B, is resisted by the conductors which are represented, for convenience, by a linear spring with stiffness K_c. On the other hand, the rotation $\Delta\theta$, is resisted by the restorative action of the vertical weight, W_g. The force-displacement relations are given in Appendix D where it is demonstrated that the conductor and insulator may be represented by two horizontal springs acting in series as shown in Figure 4.4. Assuming small displacements, the magnitude of the insulator's equivalent lateral stiffness, K_I is given by [16,20,21]

$$K_I = W_g / L_I \qquad (4.1)$$

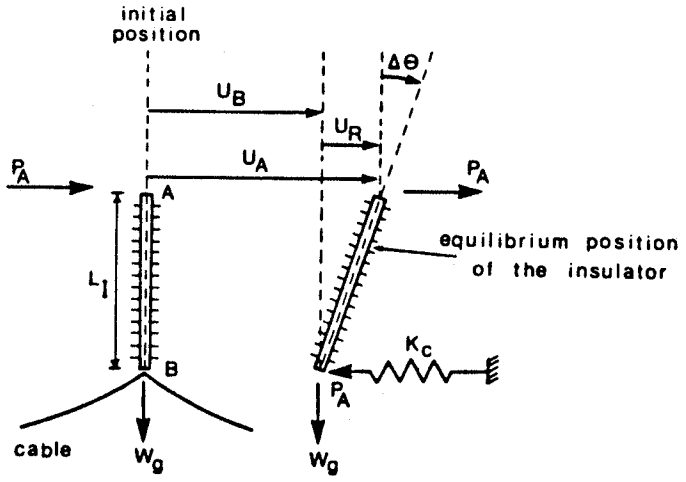

Figure 4.3: Illustrating the Derivation of the Insulator's Stiffness.

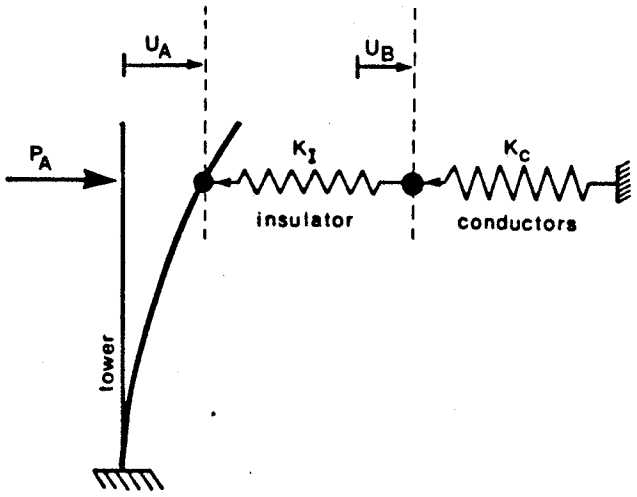

Figure 4.4: Model of the Restraint Provided by the Insulator-Conductor System.

where L_I is the length of the insulator. The representation of the stiffness K_I in the finite element model and the series connection to the conductors will be described in the next sections.

4.2.4 Conductors

Typical span and sag-tension conditions for the line are shown in Figure 4.1. A finite element modelling of the conductors was accomplished by employing the same type of elements as were used for the guys. However, only vertical galloping excitation was considered and therefore four-by-four in-plane element matrices were used to reduce computational effort. On the other hand, the conductors are very much longer than the guys. Therefore, it was suspected that long-

itudinal resonances of the conductor might occur close to the lowest natural frequencies predominantly affecting the tower. Thus, longitudinal inertia was included in the conductor elements. The insulator string was modelled by a very short beam element which cantilevers vertically from the tower. The deflections of the tip of this beam in the along-line direction represent the swing of an insulator because the cantilever stiffness ($3EI/L^3$) is made equal to K_I. In other directions the beam is essentially rigid. Also, the mass of the short beam is made identical to that of the insulator so that the modelling then conforms with the schematic representation shown in Figure 4.4.

The conductors are shown in Figure 4.1 connected at each end of their far ends to a linear spring of stiffness K_r. The purpose of these springs is to represent static coupling with remote spans. The magnitude of K_r varies with the number of spans considered [18]. Here, it has been assumed that there is one additional span at each remote end. The horizontal stiffness of one span is added, therefore, to the stiffness of the remote insulator to produce a value for K_r of 17000 N/m.

4.3 Results and Discussion

4.3.1 Trial solutions

Several finite element models were constructed to investigate the interactions amongst structural components. Furthermore, the importance of the axial loads on the tower and conductor end conditions were evaluated. Specifically, the models studied were:

a) An isolated tower and guys - no axial loads;

b) An isolated tower and guys - bending stiffness modified to account for axial loads;

c) As (b) but with conductors included - direct connection to the tower, remote ends fixed.

d) As (c) but including insulators.

e) As (d) with the far ends of the conductor coupled to remote spans through the spring stiffness K_r.

The lowest bending and torsional natural frequencies of the isolated tower were found from models (a) and (b) to occur in the range of 1.5 to 1.8 Hz. However, the lowest natural frequencies started at about 0.2 Hz in models (c), (d) and (e) and the corresponding mode shapes predominantly involve transverse vibration of the conductors in the plane of sag. Significant differences in the natural frequencies given by models (c), (d) and (e) will be discussed later.

During icy conditions the conductors can be excited to large amplitudes of vibration in the lowest frequency modes;

the phenomenon is known as galloping. In this situation the resulting tower forces may be significant. Such interactions can be calculated directly from the mode shapes by assuming a galloping amplitude from experience. Here, it is assumed that the maximum galloping amplitude is 6 metres in the fundamental or one loop (conductor) mode. This magnitude is approximately that chosen in reference [18] for a similar span length. Also, in compliance with that reference, the amplitude of the nth harmonic is assumed to be $6/n^2$ metres, according to the principal of equipartition of energy. Consequently, the maximum amplitudes for double and triple loop galloping are 1.5 and 0.67 metres, respectively. Galloping with more than 3 loops per span is a rare event and, from the above formula, amplitudes should not be significant.

4.3.2 Behaviour of the tower without conductors

4.3.2(a) Excluding out-of-plane inertia of the guys

In order to illustrate the interaction between the guy wires and the tower without confusion, the solution obtained by neglecting out-of-plane guy inertia will be considered first. Then, the six lowest natural frequencies and corresponding modes for the isolated tower are as shown in Figure 4.5. The results are from model (b) which includes axial loads. In each mode it can be seen that the guy-wires are vibrating essentially in their fundamental or one-loop mode. Indeed, all of the frequencies shown in Figure 4.5 are within 15% of the fundamental natural frequency for in-plane vibration of a guy with both ends fixed (1.72 Hz). Neverthe-

less, the tower motions are strongly dependent upon the relative phases of the four vibrating guys and the degree of interaction between the tower and the guys is significant. Depending on the direction of the four interaction forces there may be a bending, torsional or axial response of the tower's frame. It may seem unusual that there is a pair of rather similar in-plane bending modes at 1.52 Hz and 1.61 Hz and, again, a pair of out-of-plane bending modes at 1.55 Hz and 1.72 Hz. However, a close study of each modal pair showed that either the directions or the magnitude of the cable interaction forces varied significantly.

The axial loads incorporated in model (b) cause only a slight reduction in the natural frequencies of the bending modes. The maximum lowering is about 8%, as can be seen from the Table V. However, the mode shapes given in Figure 4.5 have significantly greater curvatures than those obtained from an analysis without axial loads (model (a)). This observation justifies the inclusion of the geometric stiffness matrix.

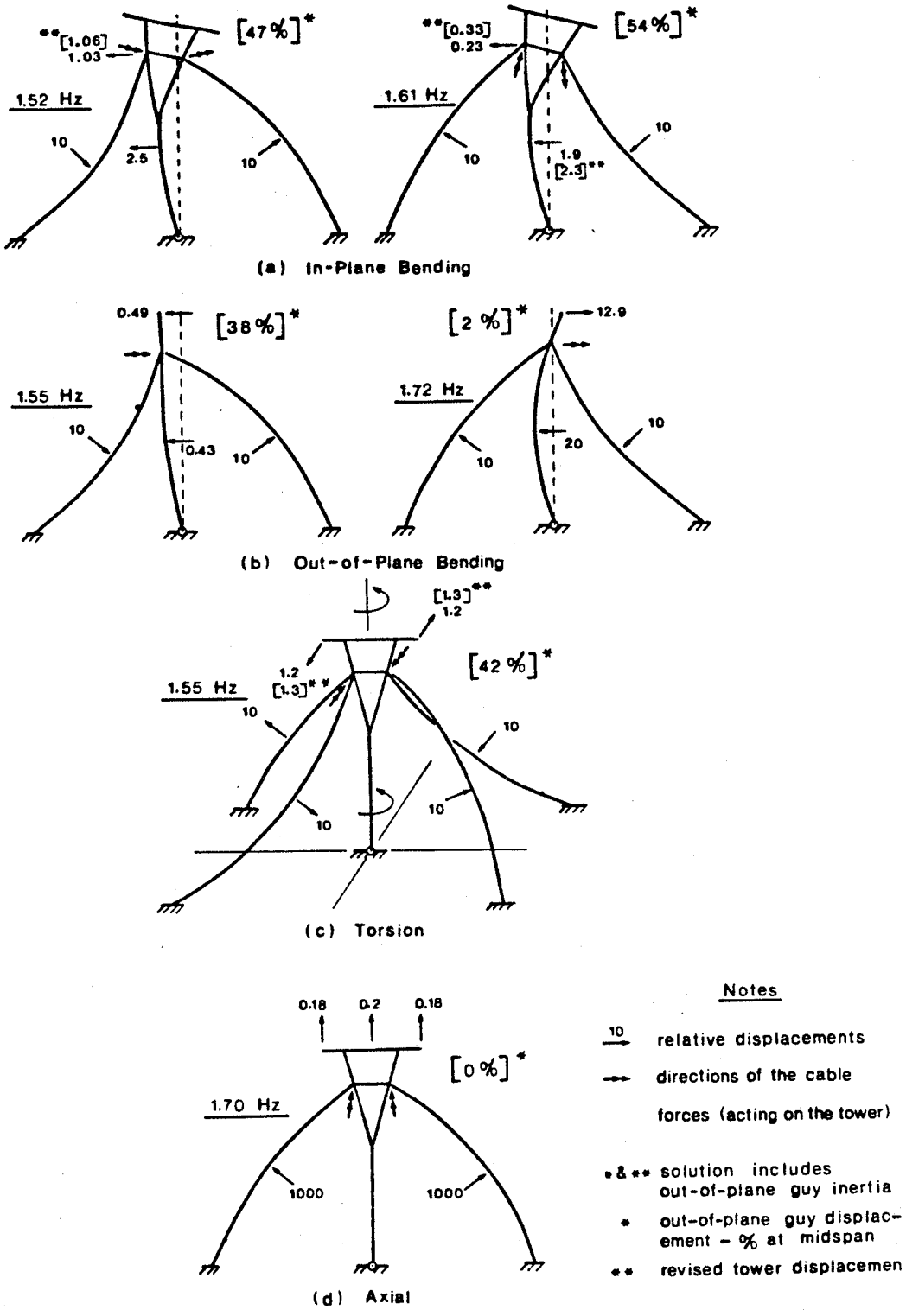

Figure 4.5: Lowest-Frequency Tower Modes from Model b.

TABLE V

Effect of Axial Loads on the Lowest Natural Frequencies Predominantly Affecting the Tower.

Mode Shape	Lowest Natural Frequencies Hz	
	Without Axial Load	With Axial Load
In-Plane Bending	1.54,1.68	1.52,1.61
Out-of-Plane Bending	1.55, 1.85	1.55, 1.72
Torsion	1.55	1.55
Axial	1.70	1.70

4.3.2(b) Including out-of-plane guy inertia:

The incorporation of the out-of-plane inertias in the guy elements produces four additional natural frequencies, as will be discussed later. However, the modes identified in Figure 4.5 are not significantly changed except that there is a coupled one-loop vibration of the guys in the out-of-plane direction. This coupling is conveniently expressed as an amplitude ratio at midspan which may be as high as 54 %. Nevertheless, the natural frequencies are unchanged. Also, the relative tower displacements are increased only slightly or not at all.

In Figure 4.6, the four additional modes are illustrated with plan diagrams because the dominant component of guy motion is out-of-plane. Indeed, all four natural frequencies occur at 1.59 Hz, which is the out-plane natural frequency of

a guy with both ends fixed. The modes are probably of less importance than those shown in Figure 4.5 because the relative magnitudes of the tower displacements are significantly smaller. Nevertheless, the diagrams in Figure 4.6 serve to illustrate the phasing of the out-of-plane guy motions associated with each type of tower displacement. Not surprisingly, it was found that the patterns shown in Figure 4.6(a),(b) and (c) also indicate the phases of the out-of-plane guy components associated with Figure 4.5(a),(b) and

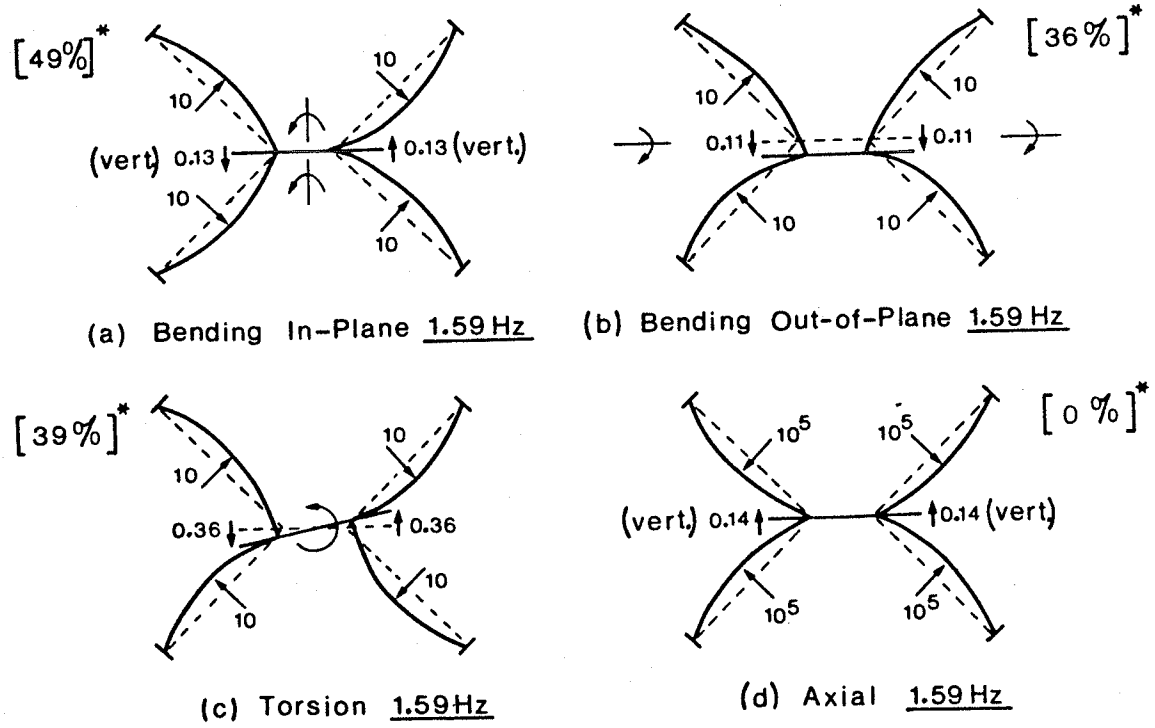

Figure 4.6: Tower Modes Coupled Predominantly with Out-of-Plane Guy Vibration.

(c), respectively.

4.3.3 Tower with conductors

The modal density for modes primarily involving transverse vibrations of the conductors is very high. There are eighteen natural frequencies shown in Table VI for the range 0.19 to 0.54 Hz. However, these frequencies can be grouped into three sets of six values depending upon whether the conductors are exhibiting one, two or three loops of vibration per span. Differences within each set depend upon the phases of the six conductor spans. This phenomenon is illustrated in Figure 4.7(a) to (f) in which the set of six single-loop modes is shown. Such modes are labelled according to the type of displacement pattern introduced by the conductors to the tower. There are three bending modes, B1, B2 and B3, a torsional mode T1, and two axial modes, A1 and A2. These types of tower response are repeated for double-and triple-loop modes as can be seen from the examples of Figures 4.7(f) and (g). Each response to conductor vibration is essentially a static deflection because the fundamental mode of the isolated tower occurs at a much higher frequency. (See Table V). This means that, in this case, the modes shown in Figure 4.7 would have been generated by representing the tower by a six-by-six array of flexibilities at the conductor attachment points. Thus, the forces and bending moments in the tower can be defined by an array of horizon-

tal translations Δ_1 through Δ_3, and vertical translations, Δ_4 through Δ_6, at the conductor attachment points. These deflections can be converted, in turn, to a set of equivalent static forces, P_1 through P_6 in Table VI, according to the flexibility of the structure. The forces were obtained by assuming appropriate galloping amplitudes as discussed previously.

A general scan of the results in Table VI shows that conditions at the conductor's end points do not significantly affect the two-loop galloping modes. This result is consistent with the theory [13,19] which shows that antisymmetric modes (2, 4 loops, etc.) occur without stretching of the cable and are not affected by conductor's longitudinal flexibility. In stark contrast, the symmetric modes (1, 3 loops, etc.) are altered significantly by the end conditions. It can be seen from Table VI(a) that if the conductors are connected directly to the tower, then the horizontal forces P_1 to P_3 for single-loop galloping are a large 10 to 15 kN. However, the inclusion of insulators in the modelling causes a reduction of these forces by a factor of about ten as shown in Tables VI(b) and (c). The corresponding natural frequencies are also reduced from 0.22 Hz to 0.19 Hz. The reduction in the vertical forces P_4 to P_6 is somewhat different. The results from Tables VI(a) and VI(b) are identical because these forces are generated without insulator swing at the central tower. However, the inclusion of static

coupling from remote spans alleviates axial stretching of the vibrating conductors as shown in Figures 4.7(d-e). Consequently, the frequencies of the one-loop modes A1, A2 and B2 are reduced from 0.30 Hz to 0.23 Hz and the forces P_4 to P_6 are attenuated by about 40%. There is a similar reduction in vertical forces resulting from the three-loop gallop, although in this case the frequencies remain unchanged at 0.54 Hz.

Table VI. Summary of Tower Loads Induced by Conductor Galloping

(a) Model (c)

Natural Freq. Hz	Horizontal Loads (N) P_1	P_2	P_3	Insu. Swing. Deg.	Tower Mode (Fig.4.7)
ONE LOOP MODES - GALLOPING AMPLITUDE = 6 m					
.22	10,083	0	-10,083	-	T1
.22	12,740	10,090	12,713	-	B1
.29	16,748	-38,109	16,758	-	B2
	Vertical Loads (N) P_4	P_5	P_6		
.30	4,954	0	4,954	-	B3
.30	4,750	-1,448	4,750	-	A1
.30	668	4,782	667	-	A2
TWO LOOP MODES - GALLOPING AMPLITUDE - 1.5 m					
	P_1	P_2	P_3		
.37	$\cong 0$	0	$\cong 0$	-	T1
.37	$\cong 0$	$\cong 0$	$\cong 0$	-	B1
.37	$\cong 0$	$\cong 0$	$\cong 0$	-	B2
	P_4	P_5	P_6		
.37	941	0	-940	-	B3
.37	938	-256	938	-	A1
.37	130	933	130	-	A2
THREE LOOPS MODES - GALLOPING AMPLITUDE = 0.67 m					
	P_1	P_2	P_3		
.53	47	0	47	-	T1
.53	44	39	44	-	B1
.54	5	-12	5	-	B2
	P_4	P_5	P_6		
.54	816	0	-816	-	B3
.54	761	-197	761	-	A1
.54	104	738	104	-	A2

(Contd.)

(b) Model (d)

Natural Freq. Hz	Horizontal Loads (N) P_1	P_2	P_3	Insul. Swing. Deg.	Tower Mode (Fig.4.7)
ONE LOOP MODES - GALLOPING AMPLITUDE = 6 m					
.19	1,532	0	-1,532	26	T1
.19	1,546	1,400	1,546	25	B1
.19	777	-1,751	777	26	B2
	Vertical Loads (N) P_4	P_5	P_6		
.30	4,962	0	-4,962	0	B3
.30	4,857	-1,370	4,857	0	A1
.30	670	4,731	670	0	A2
TWO LOOP MODES - GALLOPING AMPLITUDE - 1.5 m					
	P_1	P_2	P_3		
.37	≅0	≅0	≅0	0	*
.37	≅0	≅0	≅0	0	*
.37	≅0	≅0	≅0	0	*
	P_4	P_5	P_6		
.37	939	0	-939	0	B3
.37	951	-260	951	0	A1
.37	132	935	132	0	A2
THREE LOOPS MODES - GALLOPING AMPLITUDE = 0.67 m					
	P_1	P_2	P_3		
.53	49	0	-49	1	T1
.53	54	46	49	1	B1
.53	26	-57	26	1	B2
	P_4	P_5	P_6		
.54	830	-	-830	0	B3
.54	750	-208	570	0	A1
.54	104	738	104	0	A2

(Contd.)

(c) Model (e)

ONE LOOP MODES - GALLOPING AMPLITUDE = 6 m					
Natural Freq. Hz	Horizontal Loads (N) P_1	P_2	P_3	Insul. Swing Deg.	Tower Mode (Fig.4.7)
.19	1,477	0	-1,477	25	T1
.19	1,516	1,368	1,516	25	B1
.19	738	-1,635	738	24	B2
	Vertical Loads (N) P_4	P_5	P_6		
.23	3,017	0	-3,017	0	B3
.23	3,077	-712	3,077	0	A1
.23	417	2,928	416	0	A2
TWO LOOP MODES - GALLOPING AMPLITUDE - 1.5 m					
	P_1	P_2	P_3		
.37	≅0	≅0	≅0	≅0	*
.37	≅0	≅0	≅0	≅0	*
.37	≅0	≅0	≅0	≅0	*
	P_4	P_5	P_6		
.37	971	0	-971	0	B3
.37	919	-266	919	0	A1
.37	128	900	128	0	A2
THREE LOOPS MODES - GALLOPING AMPLITUDE = 0.67 m					
	P_1	P_2	P_3		
.53	54	0	-54	1	T1
.53	54	49	54	1	B1
.53	28	-61	28	1	B2
	P_4	P_5	P_6		
.54	672	0	-672	0	B3
.54	606	-158	606	0	A1
.54	84	602	84	0	A2

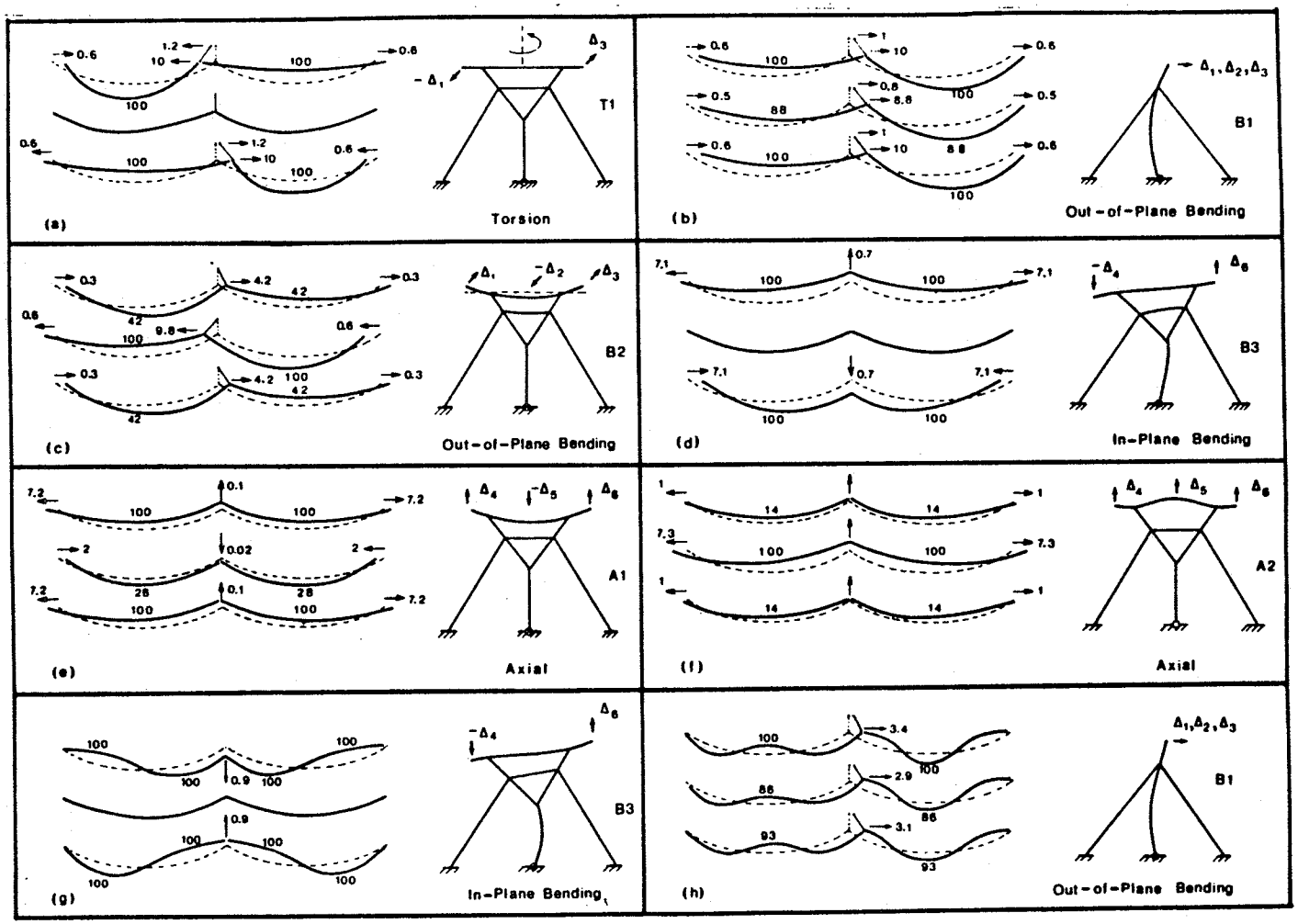

Figure 4.7: Lowest Frequency Modes and Corresponding motions of the Tower Given by Model e.

The above trends are consistent with theoretical expectations. However, an assessment of the importance of the loads is obtained most appropriately from Table VI(c) because these results were generated by using the most realistic end conditions. The galloping loads may be compared with other conductor loads such as the total weight of one span with 44 mm of radial ice (6,700 N) or a horizontal load due to a 45-m/s wind (6,200 N). In terms of these values, the galloping forces are not catastrophic by themselves. However, it should be noted that the present analysis considers the bare-wire condition, which is consistent with very light icing. A more significant comparison is the ratio of the galloping loads to the conductor's weight (3830 N per span). The fact that this ratio is significant for single-loop galloping points to the need to undertake further parametric studies. In particular, galloping may well occur under the condition of heavy icing assumed by Tsui [18]. It might be expected, then, that the galloping loads will grow approximately in proportion to the increased weight of the conductors. However, there are several additional factors. For instance, the resistance against insulator swing, represented by the spring constant K_I, will also rise with a greater weight. Furthermore, a galloping excitation may occur in one, rather than two or three, adjacent conductors. This occurrence would not necessarily be beneficial because the resulting loads would introduce coupled bending and torsion into the tower's frame.

Finally, the effect that the conductors and insulators have on those frequencies in Table V which primarily affect the tower should be elucidated. It can be seen from Table VII that the out-of-plane bending and torsional frequencies are increased slightly by the longitudinal stiffness of the conductors. However, the inclusion of the insulator swing decreases the longitudinal motion of the conductors, as shown in Figure 4.8. The frequencies corresponding to out-of-plane bending and torsion of the tower then return to the values for an isolated tower. On the other hand, the in-plane bending frequencies appear to be lowered very slightly by the inclusion of insulators and conductors. This effect was found to be due to an increase in the in-plane rotational inertia caused by (a) the mass of the insulators and (b) the lumped mass of the conductor elements which are adjacent to the cross arm. Therefore, it appears that the conductors' motions have a negligible effect on this tower's lowest modes. Nonetheless, the first resonance involving mainly longitudinal motion of the conductor was detected at 1.02 Hz and this mode is illustrated in Figure 4.9. Such modes may be important in the study of phenomena such as ice-shedding or broken-wire conditions which result in sudden changes in the conductor's tension. The appearance of this mode at a frequency lower than that of the isolated tower's fundamental mode justifies the inclusion of the longitudinal inertia in the conductor's modelling.

TABLE VII

The Effect of Insulators and Conductors on the Lowest Natural Frequencies Predominantly Affecting the Tower.

Mode	Isolated Tower	With Conductors		Insulator & End Spring
		No Insulator	Insulator	
In Plane Bend.	1.52, 1.61	1.51, 1.59	1.48, 1.56	1.48, 1.56
Out-of -Plane Bend.	1.55, 1.73	1.56, 1.94	1.55, 1.71	1.55, 1.72
Tors- ion	1.56	1.65	1.56	1.56
Axial	1.70	1.70	1.70	1.70

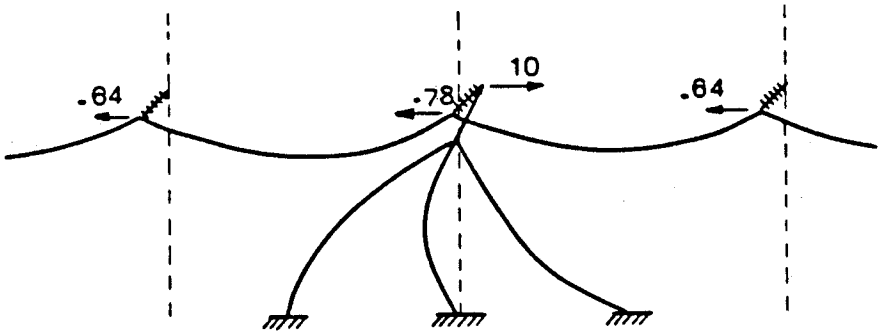

Figure 4.8: Vibration of the Transmission Line System at a Natural Frequency of 1.55 Hz.

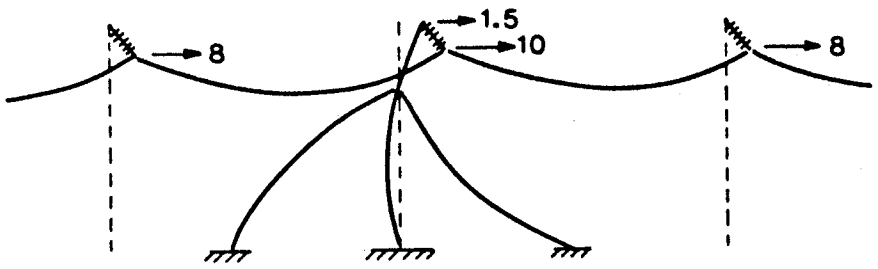

Figure 4.9: Lowest-Frequency Mode Involving a Significant Longitudinal Motion of the Conductors.

4.4 Conclusion

The free-vibration characteristics have been determined for a two-span transmission line with guyed supporting towers. Low-frequency modes essentially involve conductor motions which may be categorized, initially, according to the number of vibration loops per span. However, within each category, whether one, two, or three loops per span, six closely spaced natural frequencies were always found. This proliferation of modes happens because there are different types of coupling with the guyed towers. The coupled motions in the towers were seen to involve three types of bending, two types of axial and a torsional deformation.

Load transferred to the tower by galloping were estimated directly from the coupled mode shapes. Very high loads occur when the conductors are connected directly to the tower. However, the inclusion of insulator swing significantly de-

creases the horizontal (along-line) loads due to galloping. In contrast, vertical loads are reduced by the inclusion of coupling with remote conductor spans. The inclusion of both these ameliorating factors suggests that the loads transferred to the tower should not be catastrophic, at least for the case of light icing.

Those mode shapes primarily affecting the towers show significant dynamic interactions between the guys and the Y-shaped steel frame. However, the corresponding natural frequencies occur in the range of 1.5 to 1.8 Hz which is much higher than that possible for one- to three-loop galloping of the conductors (0.19 to 0.54 Hz). On the other hand, a longitudinal conductor resonance was identified at 1.0 Hz which is fairly close to this range. Such conductor modes may be important in the study of the dynamic response due to ice-shedding or a broken-wire condition.

Chapter V

SUMMARY AND CONCLUSIONS.

An algorithm to perform the free-vibration analysis of a tower has been developed. The basic element of the tower system can be either a lattice or a non-lattice structure. This supporting structure can be either free-standing or guy-supported. The algorithm is suitable for use on a micro-computer.

The approach is based on the assumption that the lattice segment can be represented approximately by an equivalent beam element. Corresponding stiffness and mass matrices for a straight lattice beam have been developed based on an assumed cubic polynomial. The exact displacement function was derived for a tapered beam element loaded only at its ends. This is a logarithmic function which gives much better results than the assumed cubic polynomial. Also, a finite element model has been developed for an inclined cable element assuming that the cable follows a parabolic profile when it hangs under its own weight. Furthermore, an estimation of the load transferred to a typical tower can be made if the amplitude of the vibrating conductor can be reasonably assumed.

The main conclusions obtained from the computations are summarized below:

1. The natural frequencies of a free-standing lattice tower obtained by the present finite element method are greater than those obtained by using SAPIV. Some of the difference between the present model and SAPIV is due to the stiffness modelling which is approximate as compared to the very detailed representation used with SAPIV. Also, part of the difference probably arises because a consistent mass matrix has been used here whereas SAPIV employs a lumped mass matrix.
2. An axial compressive load was incorporated by use of a geometric stiffness matrix. For the tower system shown in Figure 4.1, the use of geometric stiffness was justified because the natural frequencies of the tower were lowered by 8%.
3. Generally, the mode shapes of interest lie in the lower frequency range. In this range the cable interacts with the tower in one, two or perhaps three vibration loops. Thus, the finite element idealization which can determine accurately the first four natural frequencies of a cable should be sufficient. At least eight cable elements are necessary for this purpose.
4. Since only the first few transverse modes of a vibrating cable need to be considered in a tower inter-

action problem, the longitudinal motion can be considered quasi-static. Therefore, longitudinal inertia can be conveniently ignored.

Suggestions for Further Research - The present algorithm can further be used to perform parametric studies of tower systems. Factors such as cable mass, pre-tension in cable, cable area of cross-section can be varied and tower system response can be studied.

REFERENCES

[1] D. B. Campbell, "Unbalanced Tensions in Transmission Line." ASCE Journal of Structural Divison, Vol. 96, No. ST10, Oct. 1970.

[2] A. G. Davenport, "The Static and dynamic Behaviour of Guy Cable Under the Loading of Ice and Wind." Proceeding of the Tenth Canadian Congress of Applied mechanics, June 1985.

[3] R. W. Clough and J. Penzien, "Dynamics of Structures." McGraw-Hill Inc. 1975.

[4] A.S. Veletsos and G.R. Darbre, "Dynamic Stiffness of Parabolic Cables." Earthquake Engineering and Structural Dynamics, Vol. 11, pp. 367-401, 1983.

[5] T.Hayashikawa and N.Watanbe, "Free Vibration Analysis of Continuous Beam." ASCE Journal of Engineering Mechanics, Vol. 111, No. 5, May 1985.

[6] J. Singer, "Elements of Numerical Analysis." Academic Press Inc. 1964.

[7] P. G. S. Trainor, N. Popplewell, A. H. Shah and C. K. Wong, "A Simple Procedure for Preliminary Dynamic Analysis of Transmission Tower." Report No. G-8401 E4.19, 1984, HVDC Research Centre, University of Manitoba.

[8] R.R. Craig, Structural Dynamics. New York: John

Wiley and Sons, 1981.

[9] J. S. Przemieniecki, "Theory of Matrix Structural Analysis." McGraw-Hill Book Company, 1968.

[10] Y. F. Chin, "Static and Dynamic Behaviour of An Existing 450-kV Type E-400 Transmission Tower. " Undergraduate Thesis, University of Manitoba, 1983.

[11] A. K. Gupta, "Vibration of Tapered Beams." ASCE Journal of Structural Engineering, Vol. 111 No. 1, January 1985.

[12] S. Timoshenko, "Theory of Elastic Stability." New York: McGraw-Hill Book Co., 2nd Edition, 1960.

[13] H.M. Irvine, "Cable Structures". Cambridge Massachusetts: MIT Press 1981.

[14] M.S. Triantafyllou, "Linear Dynamics of Cables and Chains." Shock and Vibration Digest, Vol. 16, pp. 9-17 March 1984.

[15] S. E. Ramberg and O. M. Griffin, "Free Vibration of Taut and Slack Marine Cables." ASCE Journal of Structural Divison, 103(ST11), November 1977.

[16] J.D. Mozer, J.C. Pohlman and J.F. Fleming, "Longitudinal Load Analysis of Transmission Line Systems." IEEE Transactions on Power Apparatus and Systems, Vol. PAS 96, pp. 1657-65, Sept/Oct. 1977.

[17] J.D. Mozer, W.A. Wood and J.A. Hribar. "Broken Wire

Tests on a Model Transmission Line System." IEEE Transactions on Power Apparatus and Systems, Vol. PAS 100 pp. 938-947, March 1981.

[18] Y.T. Tsui, "Dynamic Behaviour of a Pylon at Chainette Line - Part I Theoretical Studies - Part II Experimental Studies." Electric Power Systems Research, Vol. 1, pp. 305-332, 1977/78.

[19] L. Kempner and S. Smith, "Cross-Rope Transmission Tower-Line Dynamic Analysis." ASCE Journal of Structural Engineering, Vol 110, pp. 1321-1335, June 1984.

[20] A.H. Peyrot, J.W. Lee, H.G. Jensen and J.D. Osteraas, "Application of Cable Elements Concept to a Transmission Line with Cross-Rope Suspension Structures," IEEE Transactions on Power Apparatus and Systems, Vol. PAS 100 pp. 3254-3262, July 1981.

[21] A. Simpson, "Determination of the Inplane Natural Frequencies of Multispan Transmission Lines by a Transfer Matrix Method," IEEE Proceedings, Vol. 113, pp. 870-878, May 1966.

Appendix A

STIFFNESS AND MASS MATRICES FOR A UNIFORM BEAM ELEMENT.

Consider a beam element with six degrees of freedom at each of its nodes. These degrees of freedom are u_1 through u_{12} as shown in Figure A1. The x-axis is in the axial direction and the y-and z-axes are principal axes in the cross-section. I_y and I_z are moments of inertia of the cross-section and I_p is the polar moment of inertia about the x-axis. The stiffness and mass coefficients associated with u_1 and u_7 are for axial deformation; those associated with u_2, u_6, u_8, and u_{12} are based on bending in the xy-plane; u_3, u_5, u_9 and u_{11} are associated with bending in the xz-plane; and u_4 and u_{10} are associated with torsion.

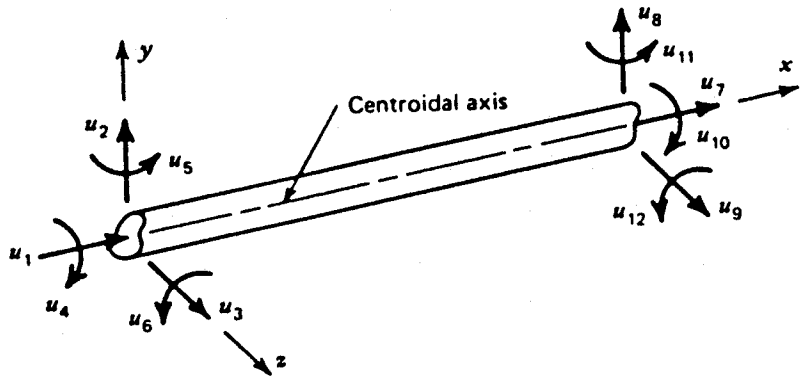

Figure A1: Notation for a beam element with 12 D.O.F.

For the beam element, shown in Figure A1, a twelve-by-twelve symmetric matrix is given in reference [8] and is as shown below.

$\frac{EA}{L}$						$\frac{-EA}{L}$						1
	$\frac{12EI_z}{L^3}$				$\frac{6EI_z}{L^2}$		$\frac{-12EI_z}{L^3}$				$\frac{6EI_z}{L^2}$	2
		$\frac{12EI_y}{L^3}$		$\frac{-6EI_y}{L^2}$				$\frac{-12EI_y}{L^3}$		$\frac{-6EI_y}{L^2}$		3
			$\frac{GJ}{L}$						$\frac{-GJ}{L}$			4
		$\frac{-6EI_y}{L^2}$		$\frac{4EI_y}{L}$				$\frac{6EI_y}{L^2}$		$\frac{2EI_y}{L}$		5
	$\frac{6EI_z}{L^2}$				$\frac{4EI_z}{L}$		$\frac{-6EI_z}{L^2}$				$\frac{2EI_z}{L}$	6
$\frac{-EA}{L}$						$\frac{EA}{L}$						7
	$\frac{-12EI_z}{L^3}$				$\frac{-6EI_z}{L^2}$		$\frac{12EI_z}{L^3}$				$\frac{-6EI_z}{L^2}$	8
		$\frac{-12EI_y}{L^3}$		$\frac{6EI_y}{L^2}$				$\frac{12EI_y}{L^3}$		$\frac{6EI_y}{L^2}$		9
			$\frac{-GJ}{L}$						$\frac{GJ}{L}$			10
		$\frac{-6EI_y}{L^2}$		$\frac{2EI_y}{L}$				$\frac{6EI_y}{L^2}$		$\frac{4EI_y}{L}$		11
	$\frac{6EI_z}{L^2}$				$\frac{2EI_z}{L}$		$\frac{-6EI_z}{L^2}$				$\frac{4EI_z}{L}$	12
1	2	3	4	5	6	7	8	9	10	11	12	

where E is the Young's modulus of elasticity; GJ is the torsional rigidity; L is the length of the element and A is the cross-sectional area of the element.

Similarly the symmetric mass matrix is as shown below:

$$\frac{mL}{420}\begin{bmatrix}
140 & & & & & & 70 & & & & & \\
 & 156 & & & & 22L & & 54 & & & & -13L \\
 & & 156 & & -22L & & & & 54 & & 13L & \\
 & & & \frac{140I_p}{A} & & & & & & \frac{70I_p}{A} & & \\
 & & -22L & & 4L^2 & & & & -13L & & -3L^2 & \\
 & 22L & & & & 4L^2 & & 13L & & & & -3L^2 \\
70 & & & & & & 140 & & & & & \\
 & 54 & & & & 13L & & 156 & & & & -22L \\
 & & 54 & & -13L & & & & 156 & & 22L & \\
 & & & \frac{70I_p}{A} & & & & & & \frac{140I_p}{A} & & \\
 & & 13L & & -3L^2 & & & & 22L & & 4L^2 & \\
 & -13L & & & & -3L^2 & & -22L & & & & 4L^2
\end{bmatrix}$$

A four-by-four geometric stiffness matrix for the axial load and corresponding to bending stiffness is as shown below

$$\begin{bmatrix}
\frac{6P}{5L} & \frac{P}{10} & -\frac{6P}{5L} & \frac{P}{10} \\
 & \frac{2PL}{15} & -\frac{P}{10} & -\frac{PL}{30} \\
\text{Symmetric} & & \frac{6P}{5L} & -\frac{P}{10} \\
 & & & \frac{2PL}{15}
\end{bmatrix},$$

in which P is the compressive axial force on the member.

Similarly a four-by-four symmetric geometric stiffness for the self weight of the element and corresponding to bending stiffness is as shown below

$$\begin{bmatrix} \frac{3\,q_o}{5} & \frac{q_o L}{10} & -\frac{3\,q_o}{5} & 0 \\ & \frac{q_o L^2}{30} & -\frac{q_o L}{10} & -\frac{q_o L^2}{30} \\ \text{Symmetric} & & \frac{3\,q_o}{5\,L} & 0 \\ & & & \frac{q_o L^2}{10} \end{bmatrix}$$

in which q_o is the self weight per unit length of the member.

Appendix B

TORSIONAL AND AXIAL STIFFNESS AND MASS MATRICES

A two-by-two stiffness matrix for an element subjected to twisting is given as

$$[K_T] = \frac{GJ}{L}\begin{bmatrix} 1 & -1 \\ -1 & 1 \end{bmatrix} \tag{B1}$$

where GJ is the torsional rigidity of the element. For a typical element, shown in Figure 2.4, GJ is as given by Equation (2.22). Also, a two-by-two mass matrix for the element is given as

$$[M_T] = m_o\begin{bmatrix} \frac{L}{3} - \frac{\beta L^2}{6} + \frac{\beta^2 L^3}{30} & \frac{L}{6} - \frac{\beta L^2}{6} + \frac{\beta^2 L^3}{20} \\ \text{Symmetric} & \frac{L}{6} - \frac{\beta L^2}{6} + \frac{\beta^2 L^3}{5} \end{bmatrix} \tag{B2}$$

where βL and m_o are as given by Equation (2.1c) and (2.23b) respectively. Similarly, a two-by-two stiffness and mass matrices for an element subjected to axial deformation is given as

$$[K_A] = \frac{EA}{L}\begin{bmatrix} 1 & -1 \\ -1 & 1 \end{bmatrix} \tag{B3}$$

in which EA is the axial rigidity of the element.

A two-by-two mass matrix is given as

$$[M_A] = \frac{mL}{6}\begin{bmatrix} 2 & 1 \\ 1 & 2 \end{bmatrix} \tag{B4}$$

in which m is the mass per unit length of the element.

Appendix C

CABLE ELEMENT STIFFNESS

The parabolic deflection of the cable shown in Figure 3.2b, at its position of static equilibrium, is given by equation [4]

$$y(x) = \frac{1}{2} \frac{q_y L_c^2}{T_o} \left[\frac{x}{L_c} - \left(\frac{x}{L_c}\right)^2\right] \tag{C1}$$

$$y'(x) = \frac{1}{2} \frac{q_y L_c^2}{T_o} \left[\frac{1}{L_c} - 2\left(\frac{x}{L_c^2}\right)\right] \tag{C2}$$

where $y(x)$ is the deflection of the cable at any point x along the chord, q_y is the intensity of the normal load per unit of chord length, L_c is the length of the chord and T_o is the component of the cable tension along the chord. The length ds of the cable element can be expressed in terms of dx and dy as

$$ds = (dx^2 + dy^2)^{1/2} \tag{C3}$$

$$\text{or} \quad ds = (1 + \frac{1}{2} y'^2)^{1/2} \, dx \tag{C4}$$

The effective cable length L_e is defined by

$$L_e = \int_o^{L_c} \left(\frac{ds}{dx}\right)^3 dx \quad . \tag{C5}$$

The static configuration of the cable is given by the differential equation [4]

$$v'' = \frac{q_y}{T_o} \frac{\Delta T_o}{T_o} \quad . \tag{C6}$$

Therefore, integrating Equation (C6) with respect to x

$$v'(x) = C'x + C_1 \tag{C7}$$

$$\text{and, } v(x) = Cx^2 + C_1 x + C_2 \tag{C8}$$

$$\text{where } C = \frac{q_y}{2} \frac{\Delta T_o}{T_o} \quad . \tag{C9}$$

C_1 and C_2 are constants of integration and can be evaluated using boundary conditions; v is the normal displacement component (in y-direction) and ΔT_o is the increment in T_o.

The equation relating the displacements and the increment in tension ΔT_o, is given by [4]

$$\Delta T_o \left(\frac{ds}{dx}\right)^3 = A_c E_c \left(\frac{\partial u}{\partial x} + \frac{\partial y}{\partial x} \cdot \frac{\partial v}{\partial x}\right). \tag{C10}$$

Combining Equations (C5) and (C10) and integrating with respect to x between the limits x_1 and x_2 for the cable element shown in Figure 3.2b yields

$$\frac{\Delta T_o}{A_c E_c} \int_{x_1}^{x_2} \left(\frac{ds}{dx}\right)^3 dx = \int_{x_1}^{x_2} du + \int_{x_1}^{x_2} \left(\frac{dy}{dx}\right) \left(\frac{v}{x}\right) dx. \tag{C11}$$

Substituting for dy/dx and $\partial v/\partial x$ from Equations (C2) and (C7) into Equation (C11)

$$\frac{\Delta T_o L'_e}{AcEc} = (u_2 - u_1) - \frac{q_y}{2T_o}\{(2x_2 - L_c)\, v_2 + (L_c - 2x_1)\, v_1\} \qquad (C12)$$

$$+ \frac{q_y}{T_o}\left\{ C_3 (x_2^3 - x_1^3) + \frac{C_3}{2}(x_2^2 - x_1^2) + C_4 (x_2 - x_1) \right\}$$

where u_1, u_2, v_1 and v_2 are displacement coordinates as shown in Figure 3.2b and L'_e is the effective length of the element, given by,

$$L_e' = \int_{x_1}^{x_2} \left(\frac{ds}{dx}\right)^3 dx \qquad (C13)$$

$$C_1 = \frac{(w_1 - w_2) - C(x_1^2 - x_2^2)}{(x_1 - x_2)} \qquad (C14)$$

$$C_2 = \frac{(w_1 x_2 - w_2 x_1) - C x_1 x_2 (x_1 - x_2)}{(x_2 - x_1)} \,. \qquad (C15)$$

Let T be the tension in the cable element and H and V be the axial and transverse components of this force along x-and y-directions, respectively. Denoting increments in the forces by prefix Δ, it can be seen that

$$H = T \cos y' \qquad (C16)$$

$$H + \Delta H = (T + \Delta T) \cos(y' + v') \qquad (C17)$$

$$V = T \sin y' \qquad (C18)$$

$$V + \Delta V = (T + \Delta T) \sin(y' + v'). \qquad (C19)$$

Considering small sags and low-amplitude motions, the cosine terms can be approximated by unity and the sine terms are equal to the quantities themselves. Neglecting higher-order non-linear terms as $\Delta T\, v'$, Equations (C16) to (C19) yield

$$\Delta H = \Delta T \qquad (C20)$$

$$\Delta V = (\Delta T \cdot y' + T\, v') \cdot \qquad (C21)$$

Considering now the case when the lower end of the cable element is restricted, ie., $u_1=v_1=0$ while the upper end moves a distance X along the x-direction ie. $v_2=0$ and $u_2=X$, Equa-

$$\frac{\Delta T\, L_e'}{A_c E_c} = X + \frac{q_y C}{T_o} \cdot \qquad (C22)$$

Combining Equations (C20) and (C22),

$$K_{xx} = \frac{\Delta H}{X} = \frac{A_c E_c}{L_e'} \left(\frac{1}{1+\rho_m}\right) \qquad (C23)$$

and $$\rho_m = \left(\frac{q_y L_c}{To}\right)^2 \frac{L_c}{L_e} \quad \frac{A_c E_c}{T_o} \quad \left(\frac{x_2 - x_1}{L_c}\right)^3 \qquad (C24)$$

where K_{xx} is the stiffness of the cable element in the x-direction. In the second case, the bottom end of the element is fixed as before while the top end is given a prescribed displacement, Y, along the y-direction, ie. $u_1=v_1=u_2=0$ and $v_2=Y$.

Substituting these boundary conditions in Equation (C13),

$$\frac{\Delta T\, L_e'}{A_c E_c} = Y\left[\frac{1}{1+\rho_m}\left\{\frac{1}{2}\frac{q_y}{T_o}(L_c - x_2 - x_1)\right\}\right]. \qquad (C25)$$

From Equations (C20) and (C25)

$$K_{xy} = \frac{\Delta H}{Y} = \frac{1}{1+\rho_m}\ \frac{A_c E_c}{L_e'}\ \left\{\frac{1}{2}\ \frac{q_y}{T_o}(L_c - x_2 - x_1)\right\} \qquad (C26)$$

where K_{xy} is the stiffness coefficient relating the force in the x-direction to the displacement in the y-direction. The expression for K_{yx}, ie., the force in the y-direction corresponding to unit displacement in the x-direction, can be obtained by relating ΔV and X. The boundary conditions in this case will be $u_1 = v_1 = u_2 = 0$ and $u_2 = X$. Applying these boundary conditions to Equation (C12) and (C21),

$$\Delta V = X\left[\frac{1}{1+\rho_m}\ \frac{A_c C_c}{L_e'}\ \left\{\frac{1}{2}\ \frac{q_y}{T_o}(L_c - x_2 - x_1\right\}\right] \qquad (C27)$$

$$K_{yx} = \frac{\Delta V}{x} = \frac{1}{1+\rho_m} \cdot \frac{A_c E_c}{L_e'}\ \left\{\frac{1}{2}\ \frac{q_y}{T_o}(L_c - x_2 - x_1)\right\}. \qquad (C28)$$

From Equations (C26) and (C28) it can be observed that $k_{xy} = k_{yx}$, which can also be justified from Maxwell's reciprocal theorem.

Finally, consider again the case when the top end is allowed to move only in the transverse y-direction, while the bottom end is fixed. The boundary conditions will be $u_1 = v_1$ $u_2 = 0$ and $v_2 = Y$. Applying these boundary conditions to Equations (C12) and (C21),

$$\Delta V = Y \left[\frac{1}{1+\rho_m} \frac{A_c E_c}{L_e'} \left\{ \frac{1}{2} \frac{q_y}{T_o} (L_c - x_2 - x_1) \right\}^2 + \frac{T_o}{x_2 - x_1} \right] \qquad \text{(C29)}$$

$$k_{yy} = \frac{\Delta V}{Y} = \frac{1}{1+\rho_m} \frac{A_c E_c}{L_e'} \left\{ \frac{1}{2} \frac{q_y}{T_o} (L_c - x_2 - x_1) \right\}^2 + \frac{T_o}{x_2 - x_1} \qquad \text{(C30)}$$

where k_{yy} is the cable force in the y-direction corresponding to a unit displacement in y-direction.

The out-of-plane stiffness, k_{zz}, of the cable element will be the same as k_{yy}. Since there is no sag in the xz-plane because of absence of any load in this plane, the term containing q_y in the expression for k_{yy} (C29) will vanish, and for the same reason $k_{zx}=k_{zy}=0$. Thus

$$Kzz = \frac{T_o}{x_2 - x_1} \quad . \qquad \text{(C31)}$$

Summary:

$$K_{xx} = \frac{\Delta H}{X} = \frac{A_c E_c}{L_e'} \left(\frac{1}{1+\rho_m} \right) \qquad \text{(C23)}$$

$$K_{xy} = K_{yx} = \frac{\Delta V}{x} = \frac{1}{1+\rho_m} \cdot \frac{A_c E_c}{L_e'} \left\{ \frac{1}{2} \frac{q_y}{T_o} (L_c - x_2 - x_1) \right\} \qquad \text{(C28)}$$

$$Kzz = \frac{T_o}{x_2 - x_1} \quad . \qquad \text{(C31)}$$

Appendix D

HORIZONTAL STIFFNESS OF AN INSULATOR

It can be seen from Figure 4.4 that the displacement due to the tower force, P_A, is U_A at the top of the insulator. However, this displacement has two components

$$U_A = U_B + U_R. \tag{D1}$$

Here U_R is a torsional component given by

$$U_R = L_I \tan \Delta\theta \tag{D2}$$

where L_I is the insulator's length. On the other hand, U_B is a translational component which depends solely upon the stiffness of the conductor spring, K_C.

The relation is obviously

$$U_B = P_A / K_C. \tag{D3}$$

Also, by resolving forces at the bottom of the insulator, it is clear that

$$P_A = W_g \tan \Delta\theta \ . \tag{D4}$$

Here W_g is the vertical load carried by the string. Substituting Equation (D4) in (D2) and rearranging gives

$$U_R = \frac{P_A}{W_g/L_I} \tag{D5}$$

where W/L may be regarded as the insulator's effective horizontal stiffness, K_I. The net stiffness at the top of the insulator may now be computed by substituting equations (D3) and (D5) into (D1) so that

$$U_A = P_A\left[\frac{1}{K_C} + \frac{1}{K_I}\right] . \tag{D6}$$

This last equation indicates a series addition of stiffness as illustrated in Figure 4.5.